HAL
archives-ouvertes.fr

Tsallis Information Measure, Multiresolution Analysis, and Nonlinear Dynamics

A. Capurro, L. Diambra, D. Lorenzo, O. Macadar, M.T. Martin, A. Plastino, Edmundo Rofman, M.E. Torres, J. Velluti

▶ **To cite this version:**

A. Capurro, L. Diambra, D. Lorenzo, O. Macadar, M.T. Martin, et al.. Tsallis Information Measure, Multiresolution Analysis, and Nonlinear Dynamics. [Research Report] RR-3184, INRIA. 1997. inria-00073505

HAL Id: inria-00073505
https://hal.inria.fr/inria-00073505

Submitted on 24 May 2006

HAL is a multi-disciplinary open access archive for the deposit and dissemination of scientific research documents, whether they are published or not. The documents may come from teaching and research institutions in France or abroad, or from public or private research centers.

L'archive ouverte pluridisciplinaire **HAL**, est destinée au dépôt et à la diffusion de documents scientifiques de niveau recherche, publiés ou non, émanant des établissements d'enseignement et de recherche français ou étrangers, des laboratoires publics ou privés.

INSTITUT NATIONAL DE RECHERCHE EN INFORMATIQUE ET EN AUTOMATIQUE

Tsallis Information Measure, Multiresolution Analysis, and Nonlinear Dynamics

A. Capurro - L. Diambra - D. Lorenzo
O. Macadar - M.T. Martin - A. Plastino
E. Rofman - M.E. Torres - J. Velluti

N° 3184
Juin 1997

THÈME 4

Les rapports de recherche de l'INRIA
sont disponibles en format postscript sous
ftp.inria.fr (192.93.2.54)

si vous n'avez pas d'accès ftp
la forme papier peut être commandée par mail :
e-mail : dif.gesdif@inria.fr
(n'oubliez pas de mentionner votre adresse postale).

par courrier :
Centre de Diffusion
INRIA
BP 105 - 78153 Le Chesnay Cedex (FRANCE)

INRIA research reports
are available in postscript format
ftp.inria.fr (192.93.2.54)

if you haven't access by ftp
we recommend ordering them by e-mail :
e-mail : dif.gesdif@inria.fr
(don't forget to mention your postal address).

by mail :
Centre de Diffusion
INRIA
BP 105 - 78153 Le Chesnay Cedex (FRANCE)

Tsallis Information Measure, Multiresolution Analysis, and Nonlinear Dynamics

Mesure d'Information de Tsallis, Analyse Multirésolution et Dynamiques non Linéaires

A. Capurro[1], L. Diambra[2], D. Lorenzo[1], O. Macadar[1],M. T. Martin[2], A. Plastino[2], E. Rofman[3], M. E. Torres[4], and J. Velluti[1].

[1] Instituto de Investigaciones Biológicas Clemente Estable, Av. Italia 3318, Montevideo, Uruguay ; E-mail : omacadar@iibce.edu.uy
[2] PROTEM (CONICET-UNLP), C. C. 727, 1900 La Plata, Argentina ;
E-mail : plastino@venus.fisica.unlp.edu.ar
[3] Institut National de Recherche en Informatique et en Automatique, Domaine de Voluceau, B. P. 105, 78153 Le Chesnay Cedex, France ; E-mail : Edmundo.Rofman@inria.fr
[4] Universidad Nacional de Entre Ríos, Depto. de Matemáticas e Informática, C. C. 57, Suc. 3, 3100 Paraná, Entre Ríos, Argentina ; E-mail : metorres@arcride.edu.ar

ABSTRACT

The present study deals with the problem of extracting information contained in complex signals. We assume that time dependent non-linear systems are the source of these signals. Two problems of choice are to be confronted, namely, i) **how** to represent the signal, i.e., in mathematical parlance, to select an appropriate basis, and ii) **which** information measure to employ. Both problems are discussed in this communication. With respect to the *first one*, we compare the classical Fourier analysis with the more modern wavelet based multiresolution one. Four different measures are confronted, in what respects to the *second choice* problem. We work with and discuss a) the orthodox Shannon one, b) the set of non-extensive Tsallis measures, c) multiresolution Shannon measures, and d) multiresolution Tsallis ones. Several applications are discussed in which diverse combinations of representation and measure are tried out. Particular attention is payed to complex signals of biological origin, with emphasis on electroencephalograms (EEG's). Our more relevant conclusion is that a Tsallis multiresolution environment appears to provide one with more detailed information than the more conventional ones.

Keywords : Wavelet Transform, Multiresolution analysis, Tsallis Information Measure, Nonlinear Systems.

Résumé

L'étude porte sur des signaux fournis par des systèmes non linéaires non stationnaires. Un analyse multirésolution où interviennent des ondelettes et la mesure d'information de Tsallis est utilisée. Plusieurs applications sont présentées. La mesure de Tsallis permette d'obtenir dans ces exemples une information plus détaillée que la mesure de Shannon.

Mots clés : Ondelettes, analyse multirésolution, mesure d'information de Tsallis, systèmes non linéaires.

Contents

List of Figures

List of Tables

I. INTRODUCTION

A. Objectives of the present communication

The last years have witnessed a systemic breakdown of the orthodox Boltzmann-Gibbs-Shannon's (BGS) statistics for systems with long-range interactions, long- time memory, or fractal space-time structure [1], which has motivated the search for possible generalizations of the BGS structures. A recent and very successful approach in this sense is the so-called generalized statistics of Tsallis, usually referred to as "Non-extensive Thermostatistics" (NET) [2,3]. In the present effort we investigate, within the generalized Tsallis framework, particular aspects of the relation between *signal analysis*, on the one hand, and *nonlinear dynamics*, on the other one. Emphasis is placed on the detection of changes in the parameters of nonlinear dynamical systems, by recourse to information gathered by analyzing experimental data, in the understanding that information measures, and particularly NET ones, should be of relevance in this endeavor.

Whenever the nonlinear dynamics can be represented by differential equations, there exist a variety of methods that provide a quantitative and qualitative characterization of the system's behavior. The spectrum of Lyapunov exponents [4], for instance, has proven to be one of the most useful dynamical diagnostic-tools for chaotic systems. For systems whose equations are explicitly known there are techniques for computing the Lyapunov spectrum [5,6]. However, in the more frequent case in which the underlying equations of the nonlinear system are not explicitly available, and one has to manage just with experimental data, these methods can not be straightforwardly applied [7]. Consequently, other approaches have been advanced that use the measured data (e.g., time series) and include the computation of the correlation dimension [8], Lyapunov exponents [7], phase space topography [9] and others. The stationarity of the signal to be analyzed is usually taken for granted. When this is definitely NOT the case, different roads are to be traversed. We intend to pave one of them in the present considerations, assuming from the outset that we have to analyze nonstationary

signals in dealing with changes in the nonlinear dynamical systems that produce our signals (the experimental data).

In reference [9], a modification of Wolf methods [7] is proposed that aims to evaluate the Lyapunov exponents by taking into account the nonstationarity of the signal. The computational cost of this method, however, is very high due to the nature of the concomitant algorithm and to the large amount of data needed. Pesin [10] has pointed out that, under some hypothesis concerning the nature of the pertinent nonlinear system, Entropic- and Lyapunov exponents-concepts become related.

We intend here to delve deeply into such entropic considerations and confront thus the following scenario: a) changes in a nonstationary signal are related to the Lyapunov exponents and b) these exponents are connected with the notion of entropy [10]. But the entropy by itself is not too useful for analyzing nonstationarities. In fact, as pointed out by Torres et al. [11], the Shannon entropy of the signal cannot always give reasonable account of changes introduced in the parameters of nonlinear models.

Looking for an improvement of the "entropy performance", Torres et al. [12,13] proposed an entropic measure with wavelet transforms that are generally acknowledged to be useful for studying nonstationary phenomena [14,15], called the *multiresolution entropy* (MRE). This MRE, a combination of the multiresolution wavelet analysis with the idea of Shannon's entropy, has been worked out and shown to provide one with an able tool for the analysis of nonstationary signals and for the detection and localization of *slight changes* in nonlinear dynamical systems [11]. This combination will here be worked out within a NET-framework.

Interestingly enough, Tsallis' entropy, and not Shannon's, will prove to be a better vehicle for our investigations. We shall present a new guise, called the *Tsallis' multiresolution entropy* (MRET), that will be shown to exhibit, as in Shannon's case [11], the following advantages : 1) over the "non-wavelet" way of computing entropies, because it is capable to detect changes in a nonstationary signal due to the localization characteristics of the wavelet transform, and 2) over the calculation of Lyapunov exponents, because the computational burden is significantly lower, since the algorithm involves only entropic computations and

uses fast wavelet transforms in a multiresolution framework.

Of course, in order to achieve our goals several additional choices must be made, once we have elected to *combine* NET tenets with Wavelet ones. We must ascertain which is the best wavelet basis, on the one hand, and which of the (in principle, infinite) different Tsallis statistics is the most suitable one for our purposes. The fact that electroencephalographic (EEG) nonstationary signals from epileptic patients are believed to possess a fractal structure makes them a suitable test-subject for our ideas.

The organization of this communication is as follows: in order to make our presentation as self-contained as possible, we devote the rest of this introductory Section to review the most important concepts of Information Theory and of Tsallis Statistical Mechanics. In the same vein, Section II is a brief review of some the multiresolution analysis concepts (and of the digital filters used for calculating the wavelet coefficients in fast form). Section III deals with the problem of evaluating the entropic content of a complex signal in a time-dependent context. A wavelet extension of the concomitant ideas and the notion of multiresolution entropy are introduced in Section IV. Examples are given in Section V. First we present nonstationary signals generated by recourse to simulations of typical nonlinear systems, with an "external" time dependent parameter. Then we deal with the results obtained with reference to a "real-life" situation, namely electroencephalographic (EEG) nonstationary signals from epileptic patients obtained using depth electrodes. Finally, some conclusions are drawn in Section VI.

B. Essential Concepts of Information Theory

It is a main contribution of Information Theory (IT) that of providing one with a recipe for mathematically ascertaining the amount of information that an observer possesses concerning a given phenomenon when only a probability distribution (PD) is known. Such an amount is referred to as an *Information Measure* (IM). The informational content of a normalized probability distribution $P(i), (i = 1, \ldots, N)$, where the subindex i runs over all

the accessible states of the relevant system is given by Shannon's IM [16]

$$H = -\sum_{i=1}^{N} P(i)\, ln[P(i)], \tag{1}$$

where the choice of the logarithm basis is used to fix the informational units. If the basis is 2 then H is measured in *bits*.

In formal fashion one is led to consider Kinchin Axioms [17] as providing the conceptual foundations of Information Theory. Consider a system Σ composed of two subsystem (Σ^1, Σ^2). Let P_i^m be a PD associated to subsystem Σ^m $(m = 1, 2)$. The PD corresponding to the total system is labelled by two subindexes i, j, one for each of the subsystem. In general, the two subsystems will be correlated. Enters here i) the conditional probability $Q(j|i)$ of finding Σ^2 in state j, when one is sure that the state of Σ^1 is that labelled by i, and ii) a concomitant *conditional* IM, expressed in terms of $Q(j|i)$. Kinchin axioms read

1) For a system Σ described by a PD $P(i)$, $i = 1, \ldots, N$, the IM is a function only of the $P(i)$

$$H\{P\} = H(P(1), \ldots, P(N)). \tag{2}$$

2) For such a system $H\{P\} \leq H\{uniformPD\}$, where the uniform PD is, of course, $P_{uniform} = \frac{1}{N}$, for all i.

3) Suppose that, instead of dealing with N states we confront $N + 1$ ones, with the proviso that $P(N + 1) = 0$. Then H remains unchanged.

4) Let Σ be composed of two subsystems, as explained above. Then

$$H(\Sigma) = H(\Sigma^1) + \sum_i P_i^1\, H\{Q|i\}. \tag{3}$$

These four axioms lead in univocal fashion to Shannon's IM (1). To most people, the first three axioms appear self-evident. However, the last one does not seem to enjoy the same status.

It may perhaps seem that a more *natural* phrasing of the fourth axiom would read

4')

$$H\{P\} = H\{P^1\} + H\{P^2\}, \tag{4}$$

but the ensuing, modified set of axioms leads not to just one but to *two* IM's. One of them is Shannon's. The other reads

$$H_{R,\beta} = (1-\beta)^{-1} ln\Big(\sum_{i=1}^{N} P_i^{\beta}\Big);\ \beta \epsilon \mathbb{R}, \tag{5}$$

which is known as Rény's IM and has found extensive applications in connection with fractals and Cantor sets [18].

Jaynes [19] has shown that if one chooses Boltzmann's constant as the informational unit and identifies Shannon's IM with the Thermodynamical entropy, then the whole of Statistical Mechanics can be elegantly reformulated, without any reference to the notion of *ensemble*, by extremalization of Shannon's H, subject to the constraints posed by the *a priori* information one may possess concerning the system of interest (the *Maximum Entropy Principle (MEP)*) [20,2]. Rény's IM cannot be regarded as a physical entropy, as it does not have a definite concavity when expressed as a function of the pertinent $P(i)$.

Can one devise an alternative version of the fourth postulate that will yield an IM of definite concavity different from Shannon's one? Assume we enact the following axiom

4")

$$H\{P\} = H\{P^1\} + H\{P^2\} + (1-q)\, H\{P^1\}\, H\{P^2\};\ q \epsilon \mathbb{R}, \tag{6}$$

which will lead to a new IM that happens to coincide with a generalized entropy recently introduced by Tsallis, inspired by multifractals [3,21,22], of the form

$$H_q = (q-1)^{-1} \sum_{i=1}^{N} [P(i) - P(i)^q], \tag{7}$$

which is related to Rény's IM $H_q(R)$ in the following fashion

$$H_q(R) = (1-q)^{-1} ln\Big(1 + (1-q)\, H_q\Big). \tag{8}$$

C. Tsallis' Generalized Statistical Mechanics

Within a classical Gibbsian context, Tsallis [6,7] showed that his entropy leads to a Generalized Statistical Mechanics (GSM). Consider a system Σ with M possible microscopic configurations and let $\{p_i\}$ stand for the probability of finding the system in the configuration i. As stated above, the associated Tsallis' IM, to be regarded here from as a physical entropy, reads

$$H_q = \frac{\sum_{i=1}^{M} (p_i - p_i^q)}{q-1}, \tag{9}$$

with q a real parameter (we have a different statistics for every possible $q-$value) and

$$\sum_i p_i = 1. \tag{10}$$

In order to study the limit $q \to 1$ we write

$$H_q = \sum_i p_i \left\{ \frac{1 - e^{(q-1)\ln p_i}}{q-1} \right\}, \tag{11}$$

and find that for $q \to 1$

$$H_1 \equiv \lim_{q-1} H_q = -k \sum_i p_i \ln p_i, \tag{12}$$

i.e., for $q = 1$ Tsallis' entropy coincides with the Gibbs-Shannon one.

¿From its definition $H_q \geq 0$ always (*positivity*)?. H_q vanishes (for all q) in the case $M = 1$, and, for $M > 1$, $q > 0$, whenever one of the p_i equals unity and the remaining ones, of course, vanish. A global, absolute maximum of H_q (for all q) obtains, according to the modified Kinchin's axioms, in the case of *equiprobability*, when all $p_i = \frac{1}{M}$. In such an instance we have

$$H_q = k \frac{M^{1-q} - 1}{1-q}, \tag{13}$$

that, in the limit $q \to 1$ leads to the celebrated Boltzmann expression

$$H_1 = k \ln M. \tag{14}$$

Tsallis' entropy exhibits a series of notable properties that reinforce the idea that H_q is indeed a physical quantity. We list some of them below.

Concavity Let us consider two PD's $\{p_i^a\}$ and $\{p_i^b\}$, where i labels the members of a set of M microstates. For a real λ such that $0 < \lambda < 1$ we define an *"intermediate" distribution* $\{p_i\}$ by recourse to

$$p_i \equiv \lambda p_i^a + (1-\lambda) p_i^b. \tag{15}$$

One easily verifies that

$$\begin{aligned} q > 0 \;&\rightarrow\; H_q[p] \geq \lambda H_q[p^a] + (1-\lambda) H_q[p^b] \\ q < 0 \;&\rightarrow\; H_q[p] \leq \lambda H_q[p^a] + (1-\lambda) H_q[p^b] \end{aligned} \tag{16}$$

The functional $H_q[p_i]$ is *concave* for $q > 0$ and *convex* for $q < 0$ (H_q being constant ($= M-1$) for $q = 0$).

Pseudo-aditivity Consider two independent systems A and B characterized by possessing M_a and M_b microstates, respectively and assume that the corresponding PD's are

$$A \longrightarrow \left\{p_1^A, p_2^A, \ldots, p_{M_a}^A\right\}, \; B \longrightarrow \left\{p_1^B, p_2^B, \ldots, p_{M_b}^B\right\}. \tag{17}$$

The total, composite system $A \cup B$ (of microstates given by all possible pairs of A- and de B-microstates) is described by the PD

$$p_{ij}^{A\cup B} = p_i^A \, p_j^B, \tag{18}$$

and one easily finds that its associated entropy is

$$H_q^{A\cup B} = H_q^A + H_q^B + (1-q) \, H_q^A \, H_q^B. \tag{19}$$

As a consequence we have

$$\begin{aligned} H_q^{A\cup B} &< H_q^A + H_q^B \;\; if \;\; q > 1 \\ H_q^{A\cup B} &> H_q^A + H_q^B \;\; if \;\; q < 1 \\ H_q^{A\cup B} &= \underbrace{H_q^A + H_q^B}_{extensivity} \;\; if \;\; q = 1 \end{aligned} \tag{20}$$

so that, except for $q = 1$, Tsallis' entropy is *a non-extensive* quantity, this being its main difference vis-a-vis the orthodox one.

Canonical ensemble Tsallis found that by extremalization of H_q under the constraints posed by both normalization and assumed knowledge of the internal energy, that is

$$\sum_{i=1}^{M} p_i = 1, \tag{21}$$

$$\sum_{i=1}^{M} p_i \varepsilon_i = U, \tag{22}$$

one obtains the generalized canonical distribution [6,7]

$$p_i^* = \frac{1}{Z_q}[1 - \beta(q-1)\varepsilon_i]^{1/(q-1)}, \tag{23}$$

where

$$Z_q^* = [1 - \beta(q-1)\varepsilon_i]^{1/(q-1)}, \tag{24}$$

is the generalized partition function.

However, more interesting results obtain if one introduces as constrain the *generalized internal energy* [7]

$$U_q = \sum_{i=1}^{M} p_i^q \varepsilon_i, \tag{25}$$

which leads to the PD

$$p_i = \frac{1}{Z_q}[1 - \beta(1-q)\varepsilon_i]^{1/(1-q)}, \tag{26}$$

with

$$Z_q = [1 - \beta(1-q)\varepsilon_i]^{1/(1-q)}. \tag{27}$$

Curado and Tsallis [7] found that the whole mathematical (Legendre-transform based) structure of thermodynamics becomes in this fashion *invariant* under a change of the $q-$value (from unity to any other real number). Indeed, one finds, for example, relations of the form

$$-\frac{\partial}{\partial\beta}\left(\frac{Z_q^{1-q}-1}{1-q}\right)=U_q, \tag{28}$$

$$\frac{\partial}{\partial U_q}\left(\frac{H_q}{k}\right)=\beta. \tag{29}$$

$$\left(\frac{Z_q^{1-q}-1}{1-q}\right)+\beta U_q=H_q, \tag{30}$$

identical to their well-known $q=1$-counterparts if one replaces $\ln Z$ by

$$\frac{Z_q^{1-q}-1}{1-q}. \tag{31}$$

One immediately realizes that

$$(H_q)\,[U_q], \quad \textit{and} \quad \left(\frac{Z_q^{1-q}-1}{1-q}\right)[\beta], \tag{32}$$

are related by a Legendre transform.

D. Generalized Entropies and Information Theory

Plastino and Plastino [23] have generalized the work of refs. [3,21,22] by 1) embedding it within a purely quantal (Hilbert space) context and 2) using Jaynes' approach to SM, which allows one to deal with (the IT equivalent of) *any* ensemble, accommodating both equilibrium and off-equilibrium situations on an equal footing.

We begin the present Section, accordingly, with some notational conventions, which are known as the Dirac ones. A vector belonging to an abstract Hilbert space is denoted by the sign

$$|\,\rangle, \tag{33}$$

which is called a *ket*, while a linear functional belonging to the associated dual space, called a *bra*, is denoted as

$$\langle\,|. \tag{34}$$

If some additional identification is needed, letter(s) are inserted within the bra's or the ket's that help to identify the vectors one is referring to. An operator, say A, acting on a Hilbert space vector is denoted as "$\hat{A}$". The internal product of two vectors $\mid a_1\rangle$ and $\mid a_2\rangle$ is denoted by $\langle a_1 \mid a_2\rangle$. In particular, we may have

$$a_2 = \hat{A} b_2, \tag{35}$$

and then we write the corresponding internal product in the fashion $\langle a_1 \mid \hat{A} b_2\rangle$. If $\hat{A}$ happens to be an Hermitian operator, the internal product is often written as $\langle a_1 \mid \hat{A} \mid b_2\rangle$. Further, if the vectors $\mid a_1\rangle$ and $\mid b_2\rangle$ *coincide* we speak of the expectation value of the (Hermitian) operator $\hat{A}$ and abbreviate it as

$$\langle \hat{A} \rangle = \langle a_1 \mid \hat{A} \mid a_1 \rangle. \tag{36}$$

The first step in addressing a purely Hilbert space context is, of course, the construction of a statistical operator (or density operator, or density matrix) $\hat{\rho}$ able to account for *all* the available information, on the one hand, and that maximizes Tsallis' entropy, on the other one. The available (a priori or prior) information can be cast in the form of a set of expectation values (EV), which are always of the form (see Eq.(36))

$$\langle \hat{A} \rangle_{q=1} = Trace(\hat{\rho}\hat{A}), \tag{37}$$

where it is understood that one has i) constructed matricial representations of the two operators above referred to, ii) multiplied the concomitant matrices, and iii) taken the Trace of the product-matrix.

Here we need, however, *generalized* EV's, in the spirit of Curado and Tsallis [22] (see above the definition of a generalized internal energy), which entails modifying the preceding formula. Within the present context we assume prior knowledge of M generalized EV's, corresponding to M (Hermitian) operators $\hat{O}_i$

$$\langle \hat{O}_i \rangle_q = Trace(\hat{\rho}^q \hat{O}_i), \quad i = 1, \ldots, M, \tag{38}$$

where, we insist, generalized EV's are being employed, according to the definition

$$\langle \hat{O}_i \rangle_q = \langle \hat{\rho}^{q-1} \hat{O}_i \rangle, \tag{39}$$

with an ordinary ($q = 1$, as in (36)) EV on the r.h.s. Of course, normalization entails

$$Tr\hat{\rho} = 1. \tag{40}$$

After a bit of algebra, recourse to that Lagrange multipliers method provides us with the normalized density operator that reproduces the M known (generalized) EV's (Cf Eq. (38)) and maximizes Tsallis' entropy. One finds [8]

$$\hat{\rho} = Z^{-1} \left(1 - (1-q) \sum_i \lambda_i \hat{O}_i \right)^{1/(1-q)}, \tag{41}$$

where Z is the partition function

$$Z = Tr \left(1 - (1-q) \sum_i \lambda_i \hat{O}_i \right)^{1/(1-q)}, \tag{42}$$

and we have M Lagrange multipliers λ_i that guarantee compliance with the M EV-related constraints. However, a small difficulty remains. The density operator is a definite positive one and, as it stands, this is not guaranteed by Eq. (41). Consequently, we must require that the operator

$$\hat{A} = 1 - (1-q) \sum_i \lambda_i \hat{O}_i, \tag{43}$$

appearing between the parenthesis in (41) be a positive definite one. This entails that the eigenvalues of $\hat{A}$ must be non-negative quantities. An ad-hoc requirement (to be justified below) is then to be introduced at this point. An heuristic cut-off is needed. Instead of (41) we write

$$\hat{\rho} = Z^{-1} \left[\hat{A}\, \Theta \left(\hat{A} \right) \right]^{1/(1-q)}, \tag{44}$$

with Z given by

$$Z = Tr \left[\hat{A}\, \Theta \left(\hat{A} \right) \right]^{1/(1-q)}, \tag{45}$$

and $\Theta(x)$ the step (Heaviside's) function

$$\Theta(x) = \begin{cases} 0 & \text{for } x \leq 0 \\ 1 & \text{for } x > 0 \end{cases} . \tag{46}$$

Equations (44- 45) should be interpreted as follows. Let $\mid i >$ and α_i, respectively, the eigenvectors and eigenvalues of the operator (43), so that (spectral decomposition)

$$\hat{A} = \sum_i \alpha_i \mid i >< i \mid, \tag{47}$$

In this special basis $\hat{\rho}$ adopts the appearance

$$\hat{\rho} = Z^{-1} \sum_i f(\alpha_i) \mid i >< i \mid, \tag{48}$$

with $f(x)$ defined according to

$$f(x) = \begin{cases} 0 & \text{for } x \leq 0, \\ x^{1/(1-q)} & \text{for } x > 0. \end{cases} \tag{49}$$

Using now the shorthand notation

$$\hat{B}' = \hat{B}\,\Theta\left(\hat{B}\right), \tag{50}$$

and

$$\hat{B} = \hat{I} - (1-q)\sum_i \lambda_i \hat{O}_i, \tag{51}$$

the generalized entropy H_q is given by

$$S_q = \frac{1}{(q-1)} Tr\left(\hat{\rho}^q \left[\hat{\rho}^{1-q} - \hat{I}\right]\right), \tag{52}$$

that is

$$H_q = \frac{1}{(q-1)} Tr\left(\hat{\rho}^q \left[Z^{q-1}\hat{B}' - \hat{I}\right]\right), \tag{53}$$

i.e.,

$$H_q = \frac{Z^{q-1}}{(q-1)} Tr\left(\hat{\rho}^q\ \hat{B}'\right) - \frac{Tr\,(\hat{\rho}^q)}{(q-1)}. \tag{54}$$

Obviously, the operators $\hat{\rho}$ and $\hat{A}$ commute. Thus, their product can be expressed in the common basis that diagonalizes them. Assuming this has been done, a bit of contemplative reflection should convince one that

$$\hat{\rho}^q \left(\hat{I} - (1-q) \sum_i \lambda_i \hat{O}_i \right) \Theta \left(\hat{I} - (1-q) \sum_i \lambda_i \hat{O}_i \right) = \hat{\rho}^q \left(\hat{I} - (1-q) \sum_i \lambda_i \hat{O}_i \right), \quad (55)$$

where, of course, all negative eigenvalues (of $\hat{A}$) have been conveniently dropped (our cut-off). With a clear conscience we can now write

$$H_q = \frac{Z^{q-1} - 1}{q-1} Tr\left(\hat{\rho}^q\right) + Z^{q-1} \sum_i \lambda_i Tr\left(\hat{\rho}^q \hat{O}_i\right) = \frac{Z^{q-1} - 1}{q-1} Tr\left(\hat{\rho}^q\right) + Z^{q-1} \sum_i \lambda_i \langle \hat{O}_i \rangle_q. \quad (56)$$

Now, from the very definition of the generalized entropy H_q we have,

$$Tr\left(\hat{\rho}^q\right) = 1 + (1-q) H_q, \quad (57)$$

so that (56) and (57) yield the *Generalized Euler's Theorem* [23]

$$H_q = \lambda_J + \sum_i \lambda_i \langle \hat{O}_i \rangle_q, \quad (58)$$

where the *Jaynes parameter* λ_J is given by

$$\lambda_j = \frac{Z^{(1-q)} - 1}{1-q}. \quad (59)$$

The parameter (59) plays, within this generalized context, the role of the logarithm of the partition function in the orthodox SM.

Generalized EV's $\langle \hat{O}_i \rangle_q$, Jaynes parameter λ_J, and the Lagrange multipliers λ_i obey certain strictures that constitute the heart of a thermodynamical description. Partial derivation of λ_J with respect to the λ_i ($i = 1, \ldots, M$) yields (consider here that our primed operator is $\hat{B} = 1 - (1-q) \sum_i \lambda_i \hat{O}_i$)

$$\frac{\partial \lambda_J}{\partial \lambda_i} = Z^{-q} \frac{\partial Z}{\partial \lambda_i}, \quad (60)$$

i.e.,

$$\frac{\partial \lambda_J}{\partial \lambda_i} = \frac{Z^{-q}}{1-q} Tr\left\{ \left[\hat{B}' \right]^{q/(1-q)} \frac{\partial}{\partial \lambda_i} \left(1 - (1-q) \sum_i \lambda_i \hat{O}_i \right) \right\}, \quad (61)$$

that is

$$\frac{\partial \lambda_J}{\partial \lambda_i} = -Z^{-q}\, Tr\left\{\left[\hat{B}'\right]^{q/(1-q)} \hat{O}_i\right\}. \tag{62}$$

which leads to

$$\frac{\partial \lambda_J}{\partial \lambda_i} = -Tr\left(\hat{\rho}^q\, \hat{O}_i\right), \tag{63}$$

that is

$$\frac{\partial \lambda_J}{\partial \lambda_i} = -\langle \hat{O}_i \rangle_q, \tag{64}$$

that, together with Euler's theorem, tell us that

$$\frac{\partial H_q}{\partial \langle \hat{O}_i \rangle_q} = \sum_{j=1}^{M} \left\{ \frac{\partial \lambda_J}{\partial \lambda_j} \frac{\partial \lambda_j}{\partial \langle \hat{O}_i \rangle_q} + \frac{\partial \lambda_j}{\partial \langle \hat{O}_i \rangle_q} \langle \hat{O}_j \rangle_q \right\} + \lambda_i, \tag{65}$$

that is

$$\frac{\partial H_q}{\partial \langle \hat{O}_i \rangle_q} = \sum_{j=1}^{M} \left\{ -\langle \hat{O}_j \rangle_q \frac{\partial \lambda_j}{\partial \langle \hat{O}_i \rangle_q} + \frac{\partial \lambda_j}{\partial \langle \hat{O}_i \rangle_q} \langle \hat{O}_j \rangle_q \right\} + \lambda_i, \tag{66}$$

and allows for the *very* important result [23]

$$\frac{\partial H_q}{\partial \langle \hat{O}_i \rangle_q} = \lambda_i. \tag{67}$$

Equations (64) and (67) constitute the basic IT relations in order to build up quantum SM à la Jaynes. In deriving them we reach the result that the whole of quantum SM is invariant under a change of q (from unity to any other real number).

The generalized EV's can be shown to obey an Ehrenfest's theorem [23]. Consider a density operator $\hat{D}(t)$ (not necessarily of the maximum entropy form) that evolves (in time) according to Von Neumann' equation

$$\frac{d\hat{D}}{dt} = \frac{1}{i\hbar}[\hat{H}, \hat{D}], \tag{68}$$

where $\hat{H}$ is the system's hamiltonian. Let $\mid \phi_i(t) >$ and α_i be, respectively, the eigenvectors and eigenvalues of $\hat{D}$. According to (68) the latter do not depend upon the time while the $\mid \phi_i(t) >$ are solutions of Schroedinger's equation

$$i\hbar \frac{d}{dt} \mid \phi_i(t) > = \hat{H} \mid \phi_i(t) > . \tag{69}$$

From the time-independent nature of the α_i one gathers that if

$$\hat{D} = \sum_i \alpha_i \mid \phi_i(t) >< \phi_i(t) \mid, \tag{70}$$

is a solution of Von Neumann's equation, another such solution is given by

$$\hat{D}^q = \sum_i \alpha_i^q \mid \phi_i(t) >< \phi_i(t) \mid . \tag{71}$$

Thus, if $\hat{D}^q$ fulfills Von Neumann's strictures, the generalized EV's $\langle \hat{O} \rangle_q$ will necessarily verify Ehrenfest's theorem [23]

$$\frac{d}{dt} \langle \hat{O} \rangle_q = \frac{1}{i\hbar} \langle [\hat{O}, \hat{H}] \rangle_q. \tag{72}$$

E. Physical Justification of Tsallis' Formalism

Plastino and Plastino [24] have justified the GSM discussed above with reference to an argument similar to that employed by Gibbs [25] himself in deriving his canonical ensemble. The idea is to go back to Gibbs' *microcanonical* ensemble (GME).

Consider a system S with energy levels denoted by ε_i, weakly interacting with a thermal bath B and assume one describes the "total" system $T = S + B$ by recourse to the GME when its total energy E lies in the interval

$$E_0 - \Delta < E < E_0 + \Delta, \tag{73}$$

with

$$\Delta << E_0. \tag{74}$$

As usual, the energy spectrum of the bath B is regarded as being of a quasi-continuous character. Plastino and Plastino [24] traverse a new road, however, in assuming that B is a *finite* system, of finite energy E_b.

As the total system T is microcanonically described, the probability p_i of finding S in a state $| i >$ of energy ε_i is proportional to the total number ν of T-configurations compatible with such a situation. In view of the quasicontinuous character of the B-energy spectrum, ν will be given by

$$\nu = 2\Delta\eta(E_0 - \varepsilon_i), \tag{75}$$

where $\eta(E)$ represents the number of states (per unit energy interval) of B in a neighborhood of E . Thus,

$$\frac{p_i}{p_j} = \frac{\eta(E_0 - \varepsilon_i)}{\eta(E_0 - \varepsilon_j)}. \tag{76}$$

Let us assume that the number of states $M(E)$ of B with energy smaller (or equal) than E grows as a power α of E. Such a growth-law is often encountered. As examples we mention

a) A set of N independent harmonic oscillators ($\alpha = N$),

b) A set of N free (nonrelativistic) particles confined in a D-dimensional box ($\alpha = DN/2$),

c) A set of N plane, rigid rotators ($\alpha = N/2$).

With this last assumption we find

$$\eta(E) \propto E^{\alpha-1}, \tag{77}$$

because $\eta(E)$ is essentially the derivative of $M(E)$ with respect to E. Thus

$$\frac{p_i}{p_j} = \frac{(E_0 - \varepsilon_i)^{\alpha-1}}{(E_0 - \varepsilon_j)^{\alpha-1}} = \frac{(1 - \varepsilon_i/E_0)^{\alpha-1}}{(1 - \varepsilon_j/E_0)^{\alpha-1}}, \tag{78}$$

so that, after multiplication by the convenient normalization factor Z^{-1}, with

$$Z = \sum_j \left(1 - \frac{\varepsilon_j}{E_0}\right)^{\alpha-1}, \tag{79}$$

we arrive at

$$p_i = Z^{-1}\left(1 - \frac{\varepsilon_i}{E_0}\right)^{\alpha-1}. \tag{80}$$

Setting

$$q = \frac{(\alpha - 2)}{(\alpha - 1)}, \tag{81}$$

and

$$\beta = \frac{(\alpha - 1)}{E_0}, \tag{82}$$

we obtain Tsallis' canonical distribution

$$p_i = Z_q^{-1}[1 - \beta(1 - q)\varepsilon_i]^{\frac{1}{(1-q)}}, \tag{83}$$

with

$$Z_q = \sum_i [1 - \beta(1 - q)\varepsilon_i]^{\frac{1}{(1-q)}}, \tag{84}$$

q being, of course, Tsallis' characteristic parameter. In the limit $q \to 1$ one recovers Gibbs' conventional expressions

$$p_i = \frac{1}{Z_1} e^{-\beta\varepsilon_i}. \tag{85}$$

$$Z_1 = \sum_i e^{-\beta\varepsilon_i}. \tag{86}$$

The physical meaning of the $q \to 1$ limit deserves special attention. So as to fix ideas let us consider that our thermal bath consists of N independent Harmonic oscillators ($\alpha = N$). Eqs. (81-82) give

$$q = \frac{(N - 2)}{(N - 1)}, \tag{87}$$

and

$$\beta = \frac{(N - 1)}{E_0}. \tag{88}$$

The limit $q \to 1$ corresponds to that situation characterized by $N \to \infty$ and $E_0 \to \infty$, the process proceeding in such a fashion as to keep constant the energy per

oscillator $W = E_0/N$. Consequently, *Tsallis' generalized canonical distribution* describes a system in thermal contact with a *finite reservoir*. Stricto sensu, infinite baths do not exist in nature, so that, in some sense, Tsallis' distribution can be regarded as the *natural* one, Gibbs' being, instead, a convenient mathematical "idealization".

The interpretation given in [24] to Tsallis GSM allows one to conclude:

1.- The values adopted by Tsallis' parameter q are determined by the nature of the appropriate thermal bath

2.- The cut-off ad-hoc condition needed so as to determine Tsallis' statistical operator appears here in a natural fashion. The probability p_i associated to the microstate $\mid i >$ vanishes whenever

$$\beta(1-q)\varepsilon_i \geq 1, \tag{89}$$

which is equivalent to the condition

$$\varepsilon_i \geq E_0. \tag{90}$$

Obviously, (90) implies $p_i = 0$: the energy of the system S cannot exceed E_0, that of the total system $T = S + B$.

F. The usefulness of Tsallis' Formalism

The last years have witnessed a systemic breakdown of the orthodox Boltzmann-Gibbs' statistics for systems with long-range interactions, long- time memory, or fractal space-time structure [1]. Instead, the generalized statistics above discussed has been able to successfully deal with these problems for which Boltzmann's fails [1].

Plastino and Plastino [26], in what constituted the first application of Tsallis' GSM to a realistic physical problem, where able to invoke the Maximization of Tsallis entropy for explaining important features of galaxy formation. Here recourse to the GSM avoided the infinities one encounters when working with the orthodox entropy.

Another striking success of GSM is that related to the relaxation of two-dimensional Euler turbulence [1]. In the relaxation of Euler turbulence several identifiable stages can be identified: an initially hollow vorticity profile develops a linear diochotron instability which saturates with the creation of long-lived vortix patches. These patches move about for hundreds of diochotron periods, shedding filaments, and eventually mixing and inwardly transporting. This process gives rise to an axisymmetric metaequilibrium state, whose density decreases monotonically with radius, which then persists for tens of thousands of diochotron periods [1]. The shape and radial vorticity profile of the metaequilibrium state is an interesting and fundamental problem. As such, one could anticipate that it could be described by a variational principle. The most natural one applying within this context is Jaynes' maximum entropy principle, using Boltzmann-Gibbs' entropy. This yields, however, highly unsatisfactory results in this case [1]. Tsallis' entropy, however, allows for the use of Jaynes' variational principle and gives, for the first time, a convincing explanation of this phenomenon, which makes it possible the construction of a comprehensive thermodynamic description of Euler turbulence [1].

II. WAVELET TRANSFORMS AND TIME-FREQUENCY ANALYSIS

A. A Review of Basic Concepts

In order to investigate the spectral properties of an analog signal $s(t)$ from its Fourier Transform (FT), full knowledge of the signal in the time-domain is required (this refers also to "future" information). In addition, if a signal suffers modifications in a small neighborhood of some temporal location, this affects the *whole* spectrum. A serious problem with the FT revolves around the impossibility of determining the beginning and the end of, for example, frequency bursts in $s(t)$. As a consequence, in several instances, such as the analysis of non-stationary signals, the Fourier transform procedure, by itself, does not provide useful information.

The lack of temporal localization in the FT is due to the fact that the underlying test functions $e^{i\omega t}$ are *periodic*, and thus not localized in any particular region of the time-axis. A possible way of surmounting this difficulty is that of Gabor [27], who introduced a time-localization "window function" $g(t-b)$, with $b \in \mathbb{R}$, where the parameter b is used to translate the window in order to cover the whole time-domain in such a fashion that one can extract local information from the Fourier transform of the signal. Gabor's transform, the so-called "short-time Fourier transform" (STFT) has rigid time-frequency windows [28] and is thus not very effective in detecting events in signals with high frequencies or for investigating signals with low frequencies.

One is then forced to look for alternatives. This led to the introduction of the "integral wavelet transform" (IWT) [29].

A "basic wavelet function" $\psi(t)$ is such that verifies [15]

$$\int_{-\infty}^{\infty} \psi(t)dt = 0. \tag{91}$$

Assume that $\psi(t) \in L^2(\mathbb{R})$ is any basic wavelet. The integral wavelet transform $W_\psi f$ of a finite energy signal $s(t)$ is defined by [15]

$$(W_\psi s)(b,a) = |a|^{-1/2} \int_{-\infty}^{\infty} s(t)\overline{\psi(\frac{t-b}{a})}dt, \tag{92}$$

where a is the scale parameter, b/a is the time-shift, and the bar indicates complex conjugation. When $a = 2^{-j}$ and $b = k\,2^{-j}$, Eq.(92) yields a *Diadyc Wavelet transform* (DWT). Thus, the DWT uses a set of variable window-sizes that are proportional to 2^{-j} and operates at all dyadic scales so as to extract information about data structures that "live" at different scales. Under appropriate conditions on $\psi(t)$, this transform can be inverted and we can get an stable reconstruction of the original signal.

There is a class of DWT that can be implemented using extremely efficient algorithms [29–31]. These types of wavelet transform are associated with mathematical structures called *multiresolution approximations of* $L^2(\mathbb{R})$ (MRA) [29,30]. The basic idea is to obtain a sequence of fine-to-coarse signal approximations by recourse to a series of successive projec-

tions on subspaces V_j of $L^2(\mathbb{R})$, which are generated from translations of a *scaling function* $\phi(t)$ at the appropriate resolution level [28,31,32]

$$V_j = \left\{ \sum_{k\in\mathbb{Z}} c_j(k)\phi_{j,k}(t),\ c_j \in l_2 \right\}, \tag{93}$$

where $\phi_{j,k}(t) = 2^{-j/2}\phi(2^{-j}t - k)$ are dilatations (or reductions) and translations of the function $\phi(t)$, referred to as the *scaling function*. Moreover, for fixed j, the set $\{\phi_{j,k}(t), k \in \mathbb{Z}\}$ must constitute an unconditional basis of V_j. The spaces V_j are also required to satisfy the additional properties

1. $... \subset V_1 \subset V_0 \subset V_{-1} \subset ...$;
2. V_0 is a closed subspace of $L^2(\mathbb{R})$;
3. $V_{-\infty} = Clos(\bigcup_{j\in\mathbb{Z}} V_j) = L^2$;
4. $V_{\infty} = \bigcap_{j\in\mathbb{Z}} V_j = \{0\}$.

Thus, a multiresolution approximation can be viewed as a "ladder" of embedded spaces. Because of the properties $(1) - (4)$, the scaling function $\phi(t)$ used to generate the MRA cannot be arbitrarily chosen. Since i) $V_1 \subset V_0$, ii) $2^{1/2}\phi(t/2) \in V_1$, and iii) $\phi(t) \in V_0$, the generating function $2^{-1/2}\phi(t/2)$ must be a linear combination of the basis $\{\phi(t-k)\}_{k\in\mathbb{Z}}$ of V_0 and

$$\phi(t/2) = 2^{1/2} \sum_{k\in\mathbb{Z}} h(k)\phi(t-k).. \tag{94}$$

This last relation is often called *the two-scale relation* or *the refinement equation*, the sequence $h(k)$ being of crucial importance in the implementation of the DWT associated with multi resolutions.

One of the basic methods for constructing wavelets involves the use of "cardinal B-spline functions" [14]. These functions are widely regarded as being the most efficient ones for both software and hardware implementation [28,33] among the set of simple possible functions with compact support.

B. Localization Problems and Polynomial Wavelet Transforms

We are now in a position to state the aims of this communication in precise fashion: we wish to deal with event localization problems within the framework of polynomial spline wavelet transforms [33]. The multiresolution representation obtained from this wavelet transform and the digital filters consequently derived will enable us to achieve an efficient time localization in the case of complex signals (such as, for instance, those resulting from EEG's epileptiform activities) in such a way that the above specified requirements are verified.

We will work with the multiresolution representation given by [33], using the compact support cubic spline $\phi(t)$ as scaling function, i.e.

$$\phi(t) = \begin{cases} 1 - |t| + (1/6)|t|^3 - (1/3)(1 - |t|)^3 & \text{if } |t| \leq 1 \\ (2 - |t|)^3/6 & \text{if } 1 \leq |t| \leq 2 \\ 0 & \text{if } |t| > 2. \end{cases} \tag{95}$$

The corresponding wavelet function $\psi(t)$ is

$$\begin{aligned} \psi(t) = \frac{1}{40320}[&-\phi(2t+6) + 124\phi(2t+5) - 1677\phi(2t+4) + \\ &+ 7904\phi(2t+3) - 18482\phi(2t+2) + 24264\phi(2t+1) - \\ &- 18482\phi(2t) + 7904\phi(2t-1) - 1677\phi(2t-2) + \\ &+ 124\phi(2t-3) - \phi(2t-4)]. \end{aligned}$$

In order to analyze the time-frequency localization properties, we calculate the values of the center and radius of the time and frequency windows, respectively, and obtain the value of the window's area in the time-frequency plane $area = 2.0013$ (almost equal to the optimal value 2, of the minimum possible window's area [28]). Thus, the selection of this wavelet guarantees a good localization in the time-frequency plane, which was the main one among the specifications of the above considerations. The numerical implementation of the pertinent algorithm will be discussed below.

The wavelet decomposition for a given signal $s(t)$, initially represented by its polynomial spline coefficients at resolution 0, is given by

$$s(t) = \sum_{k=-\infty}^{\infty} c_0(k)\phi(t-k)$$
$$= \sum_{k=-\infty}^{\infty} c_N(k)\phi(2^{-N}t-k) + \sum_{j=1}^{N}\sum_{k=-\infty}^{\infty} d_j(k)\psi(2^{-j}t-k), \quad (96)$$

where the numbers $d_1(k), d_2(k), \ldots, d_N(k)$ are the wavelet coefficients, and the sequence $\{c_N(k)\}$ represents the coarser resolution signal at resolution level N. If this decomposition is carried out over all resolutions levels, the wavelet expansion

$$s(t) = \sum_{j=-\infty}^{\infty}\sum_{k=-\infty}^{\infty} d_j(k)\psi(2^{-j}t-k), \quad (97)$$

is obtained. At each level j, the series in Eq.(97) has the property of "complete oscillation" [28], which makes the decomposition useful in applications to event-time-localizations.

At this point, it is convenient to introduce two digital filters that can be profitably used in connection with this algorithm ([33,34]). They are given by the transfer functions

$$B^{-1}(z) = \frac{6}{z+z^{-1}+4}$$
$$A^{-1}(z) = \frac{5040}{z^3+z^{-3}+2416+1191(z+z^{-1})+120(z^2+z^{-2})}$$

where z is a complex variable.

As it is usual, we indicate with $b^{-1}(k)$ and $a^{-1}(k)$ the impulse responses of these filters. Following [33,34], we employ a fast recursive scheme, for obtaining the expansion coefficients in (96). The pertinent recipe reads

$$c_0(k) = [b^{-1} * s](k) \quad (98)$$
$$c_{j+1}(k) = [v^* * c_j]_{\downarrow 2}(k) \quad (99)$$
$$d_{j+1}(k) = [w^* * c_j]_{\downarrow 2}(k),, \quad (100)$$

where

$$v^*(k) = (1/2)[[a^{-1}]_{\uparrow 2} * a * u](k) \quad (101)$$
$$w^*(k) = (1/2)[[a^{-1}]_{\uparrow 2} * u_s * \delta_1](k), \quad (102)$$

and

$$u_s(k) = (-1)^k u(k), \quad \delta_1 * a(k) = a(k-1). \tag{103}$$

The symbol * means discrete convolution, $u(k)$ is the binomial kernel corresponding to the cubic spline (of order 3), provided by the two scale relation (94), and is defined by

$$u(k) = \begin{cases} (1/2)^3 \begin{pmatrix} n+1 \\ k+(n+1)/2 \end{pmatrix} & if |k| <= (n+1)/2 \\ 0 & \text{otherwise} \end{cases} \tag{104}$$

And $[a]_{|2}(k)$ stands for $\ldots, a(-2), a(0), a(2), \ldots$, while $[a]_{|2}(k) = a(k/2)$ if k is even and $[a]_{|2}(k) = 0$ if k is odd.

We conclude this section by reiterating which is our core-procedure: the coefficients of the expansion (96) are to be computed using the digital filters (101) and (102).

III. THE ENTROPY CONCEPT AS APPLIED TO A SIGNAL

A. Preliminary Considerations

It is possible to define the entropy $H(t)$ of a signal $s(t)$ in different ways (see, for instance, [35–37] and references therein). Given the signal $s(t)$ and a time lapse $(0, T)$, what one generally considers is the entropy of the (whole) associated "s- curve" for the concomitant temporal interval. Such an entropy is not very helpful for our present endeavor. We need, instead, a *time dependent entropy* (TDE), so that previous definitions [35–37] become unsuitable. In order to devise such a TDE we need an adequate partitioning of the pertinent time-interval, which in turn can easily be accomplished by introducing the idea of a "sliding window". As proposed by Torres et al. in [11,12] in Shannon's case, by recourse to this sliding window concept we shall in what follows cast the entropic notion in a fashion that will be proven to be of utility.

Let $s(t)$ denote the temporal behavior of a given signal. It is assumed that $s(t)$ is produced by some nonlinear dynamical system. We hope to gather physical information by

studying this signal. Consider the graph "signal amplitude $s(t)$ vs. time" and a discrete-time set of amplitude values

$$D = \{s(t_k), \quad k = 1, \ldots, K\}. \tag{105}$$

In order to compute the pertinent probability distributions to be associated with the relevant data, we consider an equipartition of D with the help of an appropriate number $L \epsilon \mathbb{N}$

$$s_0 < s_1 < s_2 < \ldots < s_L, \tag{106}$$

where

$$s_0 \triangleq \min[D] = \min_k \{s(t_k), k = 1, \ldots, K\}, \tag{107}$$

and

$$s_L \triangleq \max[D] = \max_k \{s(t_k), k = 1, \ldots, K\}. \tag{108}$$

We introduce at this stage the set $\{I_l = [s_{l-1}, s_l), l = 1, \ldots, L\}$, of disjoint intervals such that

$$D = \overline{\bigcup_{l=1}^{L} I_l}. \tag{109}$$

We define now a sliding temporal window W depending on two parameters: the width $w \in \mathbb{N}$ (an even number), and the sliding factor $\Delta \in \mathbb{N}$. This sliding window (of data) is defined according to

$$W(m; w, \Delta) = \{s(t_k), k = 1 + m\Delta, \ldots, w + m\Delta\}, m = 0, 1, 2, ..., M, \tag{110}$$

where Δ and w are selected such that $w \leq K$ and $(K - w)/\Delta \in \mathbb{N}$. For example, if $w = 10$ and $\Delta = 5$, $W(0; 10, 5) = \{s(t_1), s(t_2), \ldots, s(t_{10})\}$, and $W(1; 10, 5) = \{s(t_6), s(t_7), \ldots, s(t_{15})\}$, etc. For the sake of a simpler notation we write here from $s(k) = s(t_k)$. The center of the window (110) is $s(w/2 + m\Delta)$. Thus, the window slides temporally and m "controls" the ensuing time displacement.

We will denote with $P^m(I_l)$ the probability that the signal $s(k) \in W(m; w, \Delta)$ belongs to the interval I_l. This probability is the ratio between the number of $s(k)$-values of $W(m; w, \Delta)$ found within I_l and the total number of $s(k)$-values in $W(m; w, \Delta)$.

The Shannon information measure to be associated to this probability set is now, according to the usual recipe,

$$\mathcal{S}_S(m) = -\sum_{l}^{L} P^m(I_l) \ln P^m(I_l), \tag{111}$$

while the corresponding Tsallis' one reads

$$\mathcal{S}_q(m) = (q-1)^{-1} \sum_{l=1}^{L} [P^m(I_l) - (P^m(I_l))^q]. \tag{112}$$

The notation here employed becomes necessary because, as the reader will soon appreciate, several entropies are to be studied in this Communication.

As stated above, the temporal dependence of these entropies is governed by the integer m. We will refer to both eq.(111) and eq.(112) as "usual" or "canonical" information measures (IM), so as to clearly distinguish them from the wavelet-based IM's to be introduced below.

B. Multiresolution Information Measures

As our present leit motiv, we introduce now information measures in a new guise, using wavelet parlance. As pointed out above, wavelets have interesting localization properties in the time-frequency plane. The wavelet coefficients corresponding to the level j of the multiresolution analysis are

$$D_j = \{d_j(k), \quad k = 1, \ldots, K_j\}, \tag{113}$$

and, if the total amount of data K to be analyzed can be accommodated so as to be given by a power of two, i.e. 2^N, the number of coefficients in the level j is a smaller quantity, represented by 2^{N-j}, due to the above described decimation effect.

Let us assume for simplicity a fixed resolution level and its wavelet coefficients

$$D = \{d(k), \quad k = 1, \ldots, K\}, \tag{114}$$

calculated as explained in Section II.

As promised, concepts introduced in the preceding Section are now to be translated into wavelet language (a preliminary report on the subject has been given in [11]). On the set (114) of wavelet coefficients we again define a sliding window depending on the two parameters width $w \in \mathbb{N}$ (an even number), and sliding factor $\Delta \in \mathbb{N}$, where, once more, we define the sliding window of data in the fashion

$$W(m; w, \Delta) = \{d(k), k = 1 + m\Delta, \ldots, w + m\Delta\}, \; m = 0, 1, 2, ..., M, \tag{115}$$

with Δ and w selected in such a manner that $w \leq K$ and $(K - w)/\Delta \in \mathbb{N}$. The center of the window (115) is $d(w/2 + m\Delta)$. Once again, m is a time-control and, for each window $W(m; w, \Delta)$, the partition

$$d_0 = d(m) < d_1 < d_2 < ... < d_L = D(m), \tag{116}$$

is to be considered, where

$$d(m) \hat{=} \min\left[W(m; w, \Delta)\right] = \min_k \left[\{d(k), k = 1 + m\Delta, \ldots, w + m\Delta\}\right], \tag{117}$$

and

$$D(m) \hat{=} \max\left[W(m; w, \Delta)\right] = \max_k \left[\{d(k), k = 1 + m\Delta, \ldots, w + m\Delta\}\right]. \tag{118}$$

Attention is now focused upon the set $\{I_l = [d_{l-1}, d_l), \, l = 1, \ldots, L\}$, of disjoint intervals such that

$$W(m; w, \Delta) = \overline{\bigcup_{l=1}^{L} I_l}. \tag{119}$$

We will indicate $p^m(I_l)$ the probability that the wavelet coefficient $d(k) \in W(m; w, \Delta)$ belongs to the interval I_l. This probability is the ratio between the number of wavelets coefficients of $W(m; w, \Delta)$ in I_l and the total number of wavelets coefficients in $W(m; w, \Delta)$.

We define the *Shannon's multiresolution entropy* (MRE) as

$$H_S(m) = -\sum_{l=1}^{L} p^m(I_l)\log(p^m(I_l)), \quad m = 0, 1, \ldots, M, \tag{120}$$

and Tsallis' one in the fashion

$$H_q(m) = (q-1)^{-1}\sum_{l=1}^{L}[p^m(I_l) - (p^m(I_l))^q], \quad m = 0, 1, \ldots, M, \tag{121}$$

(to be abbreviated as MRET).

MRE and MRET allow one to follow the entropy evolution (time-control m) of the wavelet coefficients at the considered resolution level. Of course, in the general case we have $M = M_j$, $D = D_j$, $K = K_j$, $L = L_j$, $W(m; w, \Delta) = W_j(m; w, \Delta)$, $p^m = p_j^m$ and $H(m) = H_j(m)$.

If we plot at each level either the MRE or the MRET vs. time, focusing our attention upon the points $\{w/2 + m\Delta, H_j(m)\}$, $m = 1, ..., M_j$, this approach possesses the localization properties of the wavelets. Thus, it should be useful in detecting parameter changes.

IV. APPLICATIONS TO DYNAMICAL MODELS

We discuss now some first applications of the formalism described in the preceding Section. We begin with the treatment of signals generated by recourse to well-known dynamical models, when one of the pertinent parameters is changed. We also report on the behavior of the MRET and of the "usual" entropy of signals obtained with constant values of the relevant parameters.

A. Henon's Map.

We start by considering a bi-parametric example in which the temporal evolution is studied with reference to the behavior of a variable x_n whose values are recorded at discrete intervals denoted by an integer figure n. The defining equations read (the parameters are called a_n and b) [38]

$$\begin{aligned} x_n &= 1 + y_{n-1} - a_n\, x_{n-1}^2 \\ y_n &= b\, x_{n-1}, \end{aligned} \tag{122}$$

and we assume a_n to be assigned either i) a fixed value 1.0623718384 (case A) or ii) a varying one, that changes according to the rule

$$a_n = \begin{cases} a_1 & \text{if} \quad n < n_1 \\ a_1 + [(n - n_1)(a_2 - a_1)/(n_2 - n_1)] & \text{if } n_1 \leq n \leq n_2 \\ a_2 & \text{if} \quad n > n_2, \end{cases} \tag{123}$$

(case B) with $a_1 = 1.062371838$, $a_2 = 1.080744879$, $n_1 = 1000$, $n2 = 1030$, while in all cases we have $b = 0.3$.

The full curve in Fig. 1 depicts x_n vs n for case A, while the dashed one is a plot of the difference

$$z_n = x_n(caseA) - x_n(caseB). \tag{124}$$

We compute now, and display in Fig. 2, Tsallis' canonical entropy for $q = 5$ using both x_n(case A) (dashed curve) and x_n(case B) (solid one) as the relevant input. Here we use, of course, the recipe of Section III in evaluating $\mathcal{S}_q$. Notice the "jump" at $n_1 = 810$. In Fig. 3, instead, we deal with MRET results, in depicting Tsallis' multiresolution information measures built up with the signals x_n (cases A and B) at three different levels. Figs. 4 and 5 are the counterparts of, respectively, Figs. 2 and 3. In the latter, however, we use Shannon's information measures. Notice that the NET entropy is a clearer indicator of the underlying dynamics' change, as a simple glance at the pertinent figures will confirm.

In all our examples we have selected small linear variations in the parameter, *that can not be detected by recourse to a mere visual inspection of the signal.*

B. Signal Generated by a Continuous Time Model.

In this example we use the celebrated Lorenz equations [38]

$$\begin{aligned} \dot{x}\,(t) &= \sigma\,[y(t) - x(t)] \\ \dot{y}\,(t) &= x(t)\,[R(t) - z(t)] - y(t) \\ \dot{z}\,(t) &= x(t)y(t) - bz(t) \end{aligned} \tag{125}$$

with parameters $\sigma = 16.0$, $b = 4.0$. $R(t)$ is used as a variable parameter that varies according to a continuous version of Eq. (123), where,*mutatis mutandis*, $R_1 = 45.92$, $R_2 = 55.92$, $t_1 = 980$ and $t_2 = 1020$. The Lyapunov spectrum for the initial value R_1 is that represented by $L_1 = 2.16$, $L_2 = 0.0$ and $L_3 = -32.4$ [7], so that we face a chaotic dynamics for the initial value R_1 of the parameter R. The Runge-Kutta method is employed with a Δt-step of 0.001 and initial values $x(0) = 10$, $y(0) = 1$, $z(0) = 0$. We compare in Fig. 6 the temporal evolution of two signals $y(t)$, namely, one (dashed line) with $R = 45.92 = constant$ and other (solid) with R varying as described above, both corresponding to the second state y. Figs. 7 and 8 depict the two ensuing Tsallis' entropies ($q = 5$), i.e. usual and MRET, while Figs. 9 and 10 display the concomitant Shannon information measures. The multiresolution results correspond in both instances to three different levels. Notice in Fig. 9 that Shannon's entropy is rather insensitive to dynamical changes. We see (bottom of Fig. 8) that the only noticeable feature of Tsallis' third-level MRET plot is *just* a valley in the region of parametric change.

V. APPLICATIONS TO BIOLOGICAL MODELS

A. Introductory Remarks

During recent years several methods of linear and nonlinear analysis has been applied to electroencephalographics (EEG) signals [37,39–43]. The community of neurophysiological researchers has understood that EEG signals stem from a highly nonlinear system [44,45,37]. Multiple feedback loops have been encountered at each of the hierarchical levels of the central nervous system. Also, individual neurons themselves appear to be highly nonlinear elements. Thus, a combination of spectral and nonlinear measures would seem to offer promissory

perspectives in undertaking EEG analysis [37]. In this communication we compare the ability of several classical and recent techniques to recognize i) the presence of large sharp waves (LSW) in turtles and ii) intercritical focal epilepsy activity (IFEA) in a given part of an EEG signal. Furthermore we will assess the efficiency of these techniques with a specific goal in mind: that of constructing an automatic device able to detect the intercritical activity in focal epilepsy. The automatic detection of epileptic spikes should be particularly valuable in this dealing with this pathology, specially when surgical treatment is indicated [46].In this work we will apply different analytic tools: Fourier Transform; Wavelets Analysis; Entropy Evolution, and Multiresolution Entropy. As discussed in the first part of the present communication, two types of entropy are to be used: Shannon's and Tsallis's. The whole weaponry enumerated above has been applied both to the EEG signal and to its derivative.

B. Biological Paradigms

The epilepsy is a medical entity characterized by recurrent seizures. In the last century [47], an English neurologist, hypothesized that the complex clinical manifestations observed during seizure are due to an excessive discharge of neuronal aggregates. This hypothesis was confirmed by Matsumoto and Ajmone-Marsan in 1964. who described the cellular correlates of the interictal and ictal manifestations [48,49]. Epileptic seizures can be partial or generalized. In partial (or focal) epilepsy the seizure begins in a restricted brain region and either remains localized or spreads to adjacent cortex. The clinical manifestations of a partial seizure reflects the region of the brain involved. From an electrophysiological point of view two types of bioelectrical signs can be distinguished in epilepsy: the interictal and the ictal activities. The interictal spike is the hallmark of the epileptiform activity and represents an intermediate epileptic state with a high degree of synchrony [50]. In the human electroencephalogram interictal epileptic spikes appear as brief (30-150 ms) negative transients with amplitudes usually ranging from 80 to 250 microvolts. The ictal activity is characterized by a sudden change in frequency where a new type of rhythm develops to dominate the tracing

[51]. This type of electrographic activity is correlated with characteristic ictal behavior. The study of the cellular basis of the interictal an ictal manifestations would be greatly facilitated by the use of an in vitro preparations. However, most in vitro preparations imply the cutting of long range neural circuits which my limit the capability to generate seizure-like activity. In turtles, the outstanding resistance to hypoxia [52] enables the isolation of large blocks of nerve tissue in vitro [53]. The electrographic activity of the in vitro brain of the turtle [53] essentially resembles that recorded in vivo [54]. The cortical field potential or corticogram of the turtle is dominated by a low-voltage ($10 - 20\ V$) non-rhythmic background activity with a distinct peak in the power spectrum around 2 to 5 Hz [55]. In 80 % of cases this background activity is randomly interrupted by spontaneous high voltage (50 to 700 V) large sharp waves or spikes. The cellular spikes correlate, is a slow, high amplitude depolarizing wave crowned by a burst of action potentials. This bioelectrical sign is similar to the paroxysmal depolarization shift described by Matsumoto and Ajmone-Marsan [48] and led us to propose that these randomly occurring spontaneous spikes could be equivalent to interictal electroencephalographic spikes.

C. Methodology

1. Signals

Digital recordings of five specimens of fresh water turtle Chrisemys D'orbigny EEGs taken from the medial cortex of a complete hemisphere in vitro have been used (300s recording for each specimen). The recordings have been performed according to the technique described in [53], with 300 Hz sample rate (150 Hz low pass filter), and with $200Hz$ sample rate (100 Hz low pass filter). The signals have been classified in 6000 samples segments with LSW and without LSW. In order to perform statistical analysis, 10 segments with LSW have been compared faced to 10 segments without LSW obtained in similar number from five turtles (sample rate 300 Hz, low pass filter 150 Hz). All compared samples had the same voltage

calibration level at the EEG ordinate scale. The human individuals digital recordings have been obtained from 5 adult patients with focal epilepsy at sleep stage 1-2 (300 seconds recording from each patient). The recordings have been obtained with a standard clinical device with 16 channels with a reference electrode placed at the patient's nose. Sample rate has been of 102.5 Hz and the low pass filter has been of 51.25 Hz. The signals have been classified in 1500 samples segments with IFEA and without IFEA. For statistical analysis purposes 20 segments with IFEA have been compared faced to 20 segments without IFEA, obtained in similar number from 5 epileptic patients. The selected segments have been recorded from the occipital, frontal, temporal and central derivations. Each pair, without IFEA and with IFEA, has been obtained from the same derivation. No significant differences have been observed in the measured magnitudes within segments without IFEA of different derivations, nor within segments with IFEA of different derivations. This fact allowed us to compare all the segments without IFEA against all the segments with IFEA mixing the distinct derivations. Furthermore, in the general statistic, the significant differences founded between segments with IFEA and without IFEA (mixing derivations) have been the same than those observed in the statistics computed separately for each derivation. As in turtle's signal cases, all samples compared had the same voltage calibration level at the EEG ordinate scale.

2. Data Processing

The EEGs of both species used have been classified in segments with spikes and without spikes for statistical comparisons purposes. Each segment has been analyzed with the following tools:

1. EEG signal (voltage as time function)

2. Fourier transform. Evaluation of the proportion of area corresponding to different frequency intervals at the spectrogram relative to the total area, have been calculated.

3. Multiresolution analysis dyadic wavelet transform at six frequency levels. Computation of the wavelet coefficients' energy at each level W_i relative to $W = W_1 + W_2 + W_3 + W_4 + W_5 + W_6$.

4. Entropy and multiresolution entropy temporal evolutions. Classic Shannon's entropy and Tsallis entropy with $q = 5$. Both entropies have been analyzed with 128 samples windows and plotted at the same time scale than the EEG signal.

5. Tools 2, 3 and 4 have been applied both to EEG signals and to their derivatives.

Statistical comparisons between the signals have been performed with the one-way ANOVA test. The significance level has been set at $P \leq 0.05$. It has been chosen in order to allow the recognition of the presence of spikes with a confidence interval of 0.95 %.

D. Results

1. Turtles

In Fig. 11, 20 s (4000 samples, sample rate 200 Hz) of turtle's EEG are shown; Fig. 11a shows an EEG segment without LSW (large sharp waves), Fig. 11b shows a segment with a clear LSW around $t = 2000$ samples. The wavelet analysis (Fig. 12) shows that this spike appears at all the scaling levels (See Fig. 12a without spike, Fig. 12b with spikes. Thus it is a complex spike: it includes components at all the frequency levels (Frequency ranges are printed above each figure). The spectrogram (Fig. 13) shows that the LSW presents a different area proportion distribution at the frequency intervals. The area corresponding to 0-15 Hz enlarges while the area corresponding to 40-100 Hz diminishes in the signal segment with LSW in comparison to the segment without LSW. Table IA shows a statistic of the observed Fourier areas changes ($n = 10$ segments, 5 turtles, sample rate 300 Hz). The observed behavior is similar to the case exemplified at Fig. 13: an enhancement in the interval 0.58-4.69 Hz and a decrease in the interval 37.5-150 Hz. The differences with

$P \leq 0.05$ are indicated with an asterisk. Some of these differences can also be accounted by the comparison of the wavelet's coefficients energy proportion at each level W_i relative to their energy sum W. In Table IB the comparison of the relative energy of each level (1-6) in segments with LSW and without LSW ($n = 10$ segments, 5 turtles, sample rate 300 Hz) is shown. The differences with $P \leq 0.05$ are indicated with an asterisk. Shannon's entropy evolution shows an abrupt fall during the LSW (Fig. 14a). Using the signal's derivative, the LSW can be detected more clearly with Shannon's entropy evolution than when applying it to the original signal (Fig. 14b). Tsallis's entropy evolution shows a clear fall during the LSW (Fig. 14c). The relation between the amplitude of this fall and the oscillations' amplitudes of this entropy at the EEG's without LSW background, results clearly greater than the one observed in Shannon's entropy case (Fig. 14a). This fact can be seen as a "sleeking" of the EEG part without LSW. The entropy fall due to the LSW is enhanced, resulting an improved detection power. Nevertheless the absolute magnitude of the entropy's fall is clearly smaller than with Shannon's entropy. Considering the signal's derivative, this fall in Tsallis's entropy during the LSW results more than 20 times enhanced. improving even more the discrimination power between the LSW and the background EEG (Fig. 14d). In the analyzed cases the derivative did not introduce false positive detections in the segment without LSW. As can be seen at Fig. 15a and Fig. 15b, the fall during the LSW appears simultaneously at the two first MRE resolution levels when applied either to the original signal or to the signal's derivative. In the analyzed segments without LSW the derivative did not introduce simultaneous falls in the entropy at several levels. The Tsallis's multiresolution entropy, applied to the original signal (Fig. 15c) as well as its derivative (Fig. 15d), clearly detects the LSW at the two first resolution levels.

2. Humans: Focal epilepsy

Fig. 16 shows the EEG of an occipital human channel, segment without intercritical epileptic activity (IFEA) (Fig. 16a) and segment with IFEA (Fig. 16b). The wavelet analysis

shows that this IFEA (intercritical focal epilepsy activity) appears at levels $W_2 - W_6$, while it is hardly detected at W_1 (Fig. 17a with IFEA and Fig. 11b without IFEA). The IFEA can also be detected by means of the wavelet's relatives energies changes along the different levels as shown in Table IIA. The segments with IFEA show a significant diminishing of the relative energy at W_1 and W_2, and a significant enhancement at W_5. The levels at which the changes are more clearly detected are W_2 (diminishing) and W_5 (enhancement). More sensibility can be obtained in certain cases by comparing the wavelet's coefficients energies addition at convenient levels. For example in this case, if we compare the segments with and without IFEA, we can appreciate that the former has less relative energy at levels $W_1 + W_2$, and a higher relative energy at levels $W_3 + W_4 + W_5 + W_6$. These changes can also be accounted at the spectrogram: the segment with IFEA has a higher area proportion in the interval 0-12.8 Hz (related to levels $W_3 + W_4 + W_5 + W_6$), and a lower one in the interval 12.8-50 Hz (related to levels $W_1 + W_2$) than the segment without IFEA (Table IIB). The differences with $P \leq 0.05$ are indicated with an asterisk. In respect of the differences observed in the spectrogram areas and wavelet coefficients energies, the use of the signal's derivative enhanced only slightly the detection sensibility of the changes mentioned above. The frequency intervals in which the differences have been more clear resulted to be shifted to higher frequency values, for example, the segment with IFEA has a bigger area in the interval 3.2-12.8 Hz of the spectrogram (related to W_3 y W_4) and a smaller one in the interval 25.6-50 Hz (related to W_1) than the segment without IFEA (Table IIIA and Table IIIB). As above, the differences with $P \leq 0.05$ are indicated with an asterisk.

Shannon's evolution entropy shows abrupt falls during the IFEA (Fig. 18a). As shown at Fig. 18b), the IFEA can be detected more clearly by means of Shannon's entropy evolution performed over the signal's derivative, than while using the original signal. It does not introduce false positive detections in the segment without IFEA. Tsallis's evolution entropy presents a clear fall during the IFEA (Fig. 18c). The relation between this fall amplitude and the entropy oscillations' amplitude in the EEG without IFEA background, results greater than in the Shannon's entropy case (Fig. 18a). Once more, this effect can be seen as a

"sleeking" of the EEG portion without IFEA, while the entropy fall due to the IFEA is enhanced, resulting an improved detection power. Nevertheless the absolute magnitude of the entropy fall is clearly smaller than with Shannon's entropy. Considering the signal's derivative, the fall in Tsallis's entropy during the IFEA results more than 20 times enhanced, improving even more the discrimination power between the IFEA and the background EEG (Fig. 18d). In the analyzed cases the derivation did not introduce false positive detection in the segment without IFEA.

As can be appreciated at Fig. 19a, the fall during the LSW appears simultaneously at the two first MRE analysis levels while applied to the original signal. The MRE of the signal's derivative (Fig. 19b) also detects IFEA with more sensibility, nevertheless the difference is not as clear as in the Shannon's entropy evolution case.

Tsallis's multiresolution entropy clearly detects the LSW at the two first levels, while applied both to the original signal (Fig. 19c) and to its derivative (Fig. 19d).

E. Results Discussion

The IFEA detection can be performed by means of the falls localization at the two first levels at Tsallis multiresolution entropy, and at the Tsallis evolution entropy of the signal's derivative. This phenomenon is not specific of the focal epilepsy, these falls in Tsallis entropy also occur in the spikes of generalized epilepsy EEG. Furthermore the relative areas in the frequency intervals 0-12.8 Hz and 12.8-50 Hz of the spectrogram, and the wavelet coefficients relative energies at levels W_2 (diminishing), and W_5 (increasing), can also be useful as detection criteria. The low standard deviations values in Tables IIA and B indicate that, within the considered population of patients with focal epilepsy disease, the changes observed in relative wavelet coefficients energy and the spectrogram areas are highly homogeneous. Thus, all the comparisons performed between segments without IFEA-with IFEA have showed a similar redistribution of wavelet relative energies. We hypothesize that the changes observed at these particular three wavelet coefficients levels might be a specific

feature of the focal epilepsy; in order to confirm this hypothesis, a larger EEGs samples analysis will be perform. The enhancement at W_5 occurs because the IFEA contains higher energy at this frequency range. Since abnormal spatio-temporal synchronizations of big populations of neurons are believed to be the underling phenomenon of the epilepsy spikes [48,49,51] the wavelet coefficients' energy diminution at levels W_1 and W_2 may be due to the lack of the normal functional activity of some part of the neuronal population recruited in the spikes. This does not mean the conservation of the total energy between the signal without IFEA and with IFEA. In fact the total energy is clearly enhanced in the signal with IFEA. Similarly, in the case of turtle's signals, the enhancement at level W_6 occurs because the EFS contains higher energy at this frequency range, and the decrease at level W_1 may be due to the lack of the normal functional activity of some part of the neuronal population recruited in the LSW.

As stated above, our ultimate aim is that of devising an automatic methods for the intercritical activity in focal epilepsy detection. The results obtained encourage us in the idea that it should be possible to design such a detector, but a larger amount of signals should have to be analyzed in order to obtain a better estimate of the confidence of the methods here proposed.

VI. CONCLUSIONS

In the present effort we have presented a new method, based in an appropriate mix of Multiresolution and Entropy Based methods, in order to perform elaborated analysis of complex signals generated by nonlinear dynamical systems.

The main idea is that of being in a position to generate, from a given complex signal, a suitable probability set, which has been accomplished in Section III. Once the probabilities are determined, Shannon's and Tsallis entropies are computed according to the pertinent definitions. The ensuing information measures have been here called the usual, or canonical ones.

Multiresolution analysis affords one the possibility of introducing a different, and perhaps more elaborate, information measure, that naturally incorporates all the advantages of wavelet analysis. In Section IV both Shannon and Tsallis multiresolution entropies are defined. With reference to well-known dynamical systems one sees that both entropies are able to detect changes in the dynamics. However, Tsallis' one seems to be the more sensitive (larger accompanying amplitude variations) one. In addition, our algorithms require smaller amounts of data samples than other procedures (e.g., those of the Lyapunov sorts).

The four ensuing information measures have been applied in analyzing the outputs of diverse nonlinear systems in Section V. It has been clearly shown that Tsallis nonextensive measures provide one with considerably more detailed information than their Shannon counterparts.

We conclude by pointing out that application of nonextensive information measures to the analysis of complex signals should receive renewed impetus from the present considerations.

VII. ACKNOWLEDGMENTS

The authors are indebted to Prof. C. D'Attellis for providing them with his filter algorithms. Sincere thanks are due to Dr. P. Flandrin and his Signal Treatment Team of the Ecole Normal Superieure de Lyon, for fruitful discussions. Comments from L. Gamero, E. Fernández and C. Mostaccio are also appreciated.

---

[1] B. M. Boghosian, Phys. Rev. E. (1996)

[2] E. T. Jaynes in *Statistical Physics*, ed. W. K. Ford, Benjamin, NY (1963).

[3] C. Tsallis, Fractals **6** (1995) 539, and references therein.

[4] V. I. Oseledec, Trudy Mosk.Mat.Obsc.**19** (1968) 179.

[5] G. Benettin, L. Galgani and J.M. Strelcyn, Meccanica **15** (1960) 9.

[6] I. Shimada and T. Nagashima, Prog. Thor. Phys. **61** (1979) 1605.

[7] A. Wolf, J. B. Swift, H. L. Swinney, Physica D **16** (1985) 285.

[8] J. Van Neerven, Master's thesis. Dept. Exp. Zoology, Univ. of Amsterdam, Amsterdam, 1988 (unpublished).

[9] L. D. Iasemidis, J. C. Sackellares, H. P. Zaveri, and W. J. Williams, Brain Topogr., **2** (1990) 187.

[10] Y. B. Pesin, Russ. Math. Surv. **32** (1977) 4; 75.

[11] M. E. Torres, L. G. Gamero, and C. E. D'Attellis, INRIA Rapp. de Rech., Prog. 5, **2812**, (Feb. 1996).

[12] M. E. Torres, L. G. Gamero, and C. E. D'Attellis, in "Proc. 1995 IEEE Workshop on Nonlinear Signal and Image Processing", Neos Marmaras-Greece, Vol. II. (Jun. 1995) 791.

[13] M. E. Torres, L. G. Gamero, and C. E. D'Attellis, Latin American Applied Research, **25** (1995) 53.

[14] C. K. Chui, *Wavelets: A tutorial in theory and applications*, Academic Press, Boston (1991).

[15] Y. Meyer, *Wavelets. Algorithms and applications* SIAM, NY (1993).

[16] C. Shannon and W. Weaver, *The Mathematical Theory of Communication*, University of Illinois Press, Urbana (1948)

[17] A. I. Kinchin, A.I., *Mathematical Foundations of Information Theory*, Dover Publ., New York (1957).

[18] A. Renyi, in "Proc. Fourth Berkeley Symposium on Math. Stat. and Prob.". Vol.1, 1970, pp547-553.

[19] E. T. Jaynes , *Information Theory and Statistical Mechanics*, Brandeis Lectures **3**. 181 (1962).

[20] A. Katz, *Principles of statistical mechanics*, Freeman, San Francisco, 1967.

[21] C. Tsallis, J. Stat. Phys.,**52** (1988) 479.

[22] E.M.F. Curado and C. Tsallis, J. Phys. A, **24** (1991)

[23] A. R. Plastino and A. Plastino, Phys. Lett. A, **177** (1993) 177.

[24] A. R. Plastino and A. Plastino, Phys. Lett. A, **193** (1994) 140.

[25] W. Gibbs, *Principles of Statistical Mechanics*, Dover, NY, 1964.

[26] A. R. Plastino and A. Plastino, Phys. Lett. A, **174** (1993) 384.

[27] D. Gabor, J. IEEE (*London*) **93** (1946) 429.

[28] C. K. Chui, *An Introduction to Wavelets*, Academic Press, NY (1992).

[29] S. Mallat, Trans. Am. Math. Soc., **315(1)** (1989) 69.

[30] S. Mallat, IEEE Trans. Signal Proc., **II** (7) (1989) 674.

[31] P. Abry and A. Aldrouby, J. Fourier Anal. Appl. (submitted)

[32] A. Aldroubi, in *Wavelets in Medicine and Biology*, ed. by A. Aldroubi and M. Unser, CRC Press, NY, Chap. I, pp 3-36 (1996).

[33] M. Unser, A. Aldroubi, and E. Murray, Signal Processing **30** (1993) 141.

[34] C. D'Attellis, S. Isaacson, and R. Sirne (private communication).

[35] P. Grassberger and I. Procaccia, Phys. Rev. A **28** (1983) 2591.

[36] A. Plastino, L. Rebollo, and G. Alvarez, Phys. Rev. A **40** (1989) 1644.

[37] J. Fell, J. Roeschke, K. Mann, and C. Schaeffner, EEG and Clin. Neurophys. **98** (1996) 401 .

[38] J. M. Thompson and Stewart, *Non linear Dynamics and Chaos*, Wiley and Sons, NY (1993).

[39] Theiler,J. and Rapp P. E.. Electroencephalography and clinical Neurophisiology **98** (1996).

213-222.

[40] C.J. Stam, T.C.A.M. van Woerkon, and W.S.Pritchard. Electroencephalography and clinical Neurophisiology **99** (1996) 214-224.

[41] Pijn, J.P., van Neerven, J., Noest, A. and Lopes da Silva. F.H., Electroencephalography and clinical Neurophisiology **79** (1991) 371-381.

[42] Anokhin, A.P., Birbaumer, N., Lutzenberger, W., Nikolaev, A., and Vogel, F. Electroencephalography and clinical Neurophisiology **99** (1996) 63.

[43] Arle, J.E. and Simon, R.H.. Electroencephalography and clinical Neurophisiology **75** (1990) 296.

[44] Rombouts, S.A.R.B, Keunen, R.W.M. and Stam, C.J.Phys. Lett. A **202** (1995) 352.

[45] Pritchard, W.S., Duke, D.W. and Krieble, K. K., Psycophysiology, **32** (1995) 486.

[46] Gotman, J., Burgess, R.C., Darcey, T.M., Herner, R.N., Ives, J.R.., Lesser, R.P., Pijn, J.P.M., and Velis, D. *Computer Applications. Surgical Treatment of the Epilepsies*, Second Edition, Ed. J. Engel, Jr. Raven Press, Ltd., New York, 1993.

[47] Jackson, J. Hughling, Br. Med. J., 1 (1890) 765.

[48] Matsumoto, H. and Ajmone-Marsan, C., Exp. Neurol., 9 (1964a) 286.

[49] Matsumoto, H. and Ajmone-Marsan,C., Exp. Neurol., 9 (1964) 305.

[50] Johnston, D. and Brown, T.H. *Electrophysiology of epilepsy.* Ed .P.A. Schwartzkroin and H.V. Wheal, Academmic Press, London, (1984) 277.

[51] Niedermeyer, E. *Electroencephalography, Basic principles, Clinical Applications and Related Field.* Niedermeyer, E. and Lopez Da Silva (eds.). F. Urban and Schwarzenberg. Baltimore, Munich. (1983) 115.

[52] Ultsch, G.R. and Jackson, D.C. J. Exp. Biol., **96** (1982) 1.

[53] Velluti, J.C., Russo, R.A., Simini, F. and García-Austt, E. Brain Behav. Evol., **38** (1991) 7.

[54] Gaztelu, J.M., García-Austt, E. and Bullock, T.H. Brain Behav. Evol. **37** (1991) 144.

[55] Velluti, J.C., Russo, R.A., Simini, F. and Garca-Austt, E. Brain Behav. Evol., 38 (1991) 7.

VIII. FIGURES AND TABLES

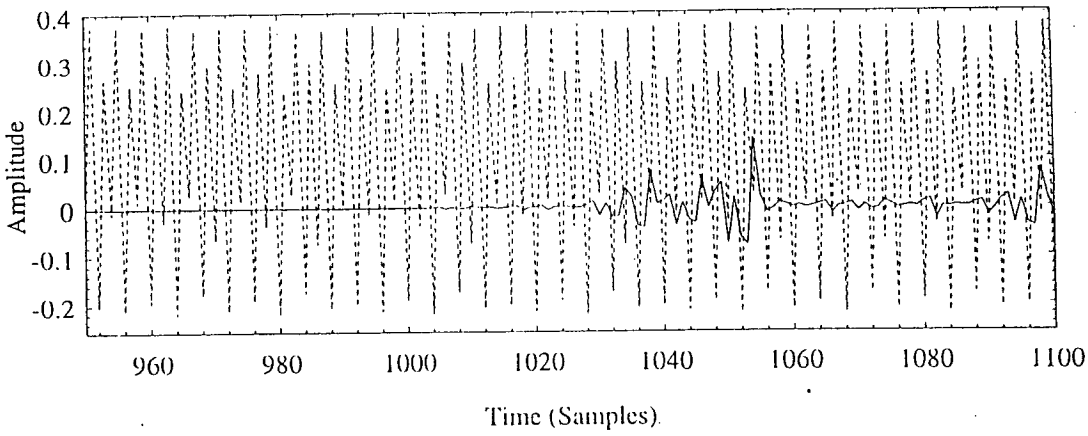

FIG. 1. Henon Map. Temporal evolution of the first state (Cf.Eq. (122)) obtained with fixed parameters $a = 1.062371838384$ and $b = 0.3$ (full line) vs. the difference between the same state and that obtained with one variable parameter as in Eq.(123)(dashed line).

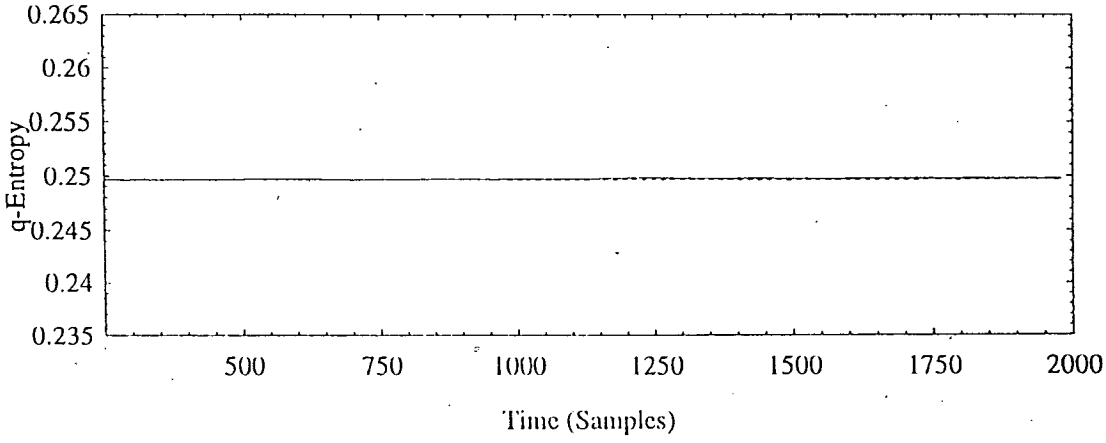

FIG. 2. Henon Map. Temporal evolution of Tsallis Entropy ($q = 5$) for the first state of equation (122) with fixed parameters (dashed line) vs. that obtained for the signal with a variable parameter (full line) (For additional details, see Fig. 1).

FIG. 3. Henon Map. Temporal evolution of the q = 5-Tsallis based Multiresolution Entropy (first three levels) for the first state of Eq. (122) with fixed parameters (dashed line) vs. that obtained for the signal with a variable parameter (full line) (For additional details, see Fig. 1).

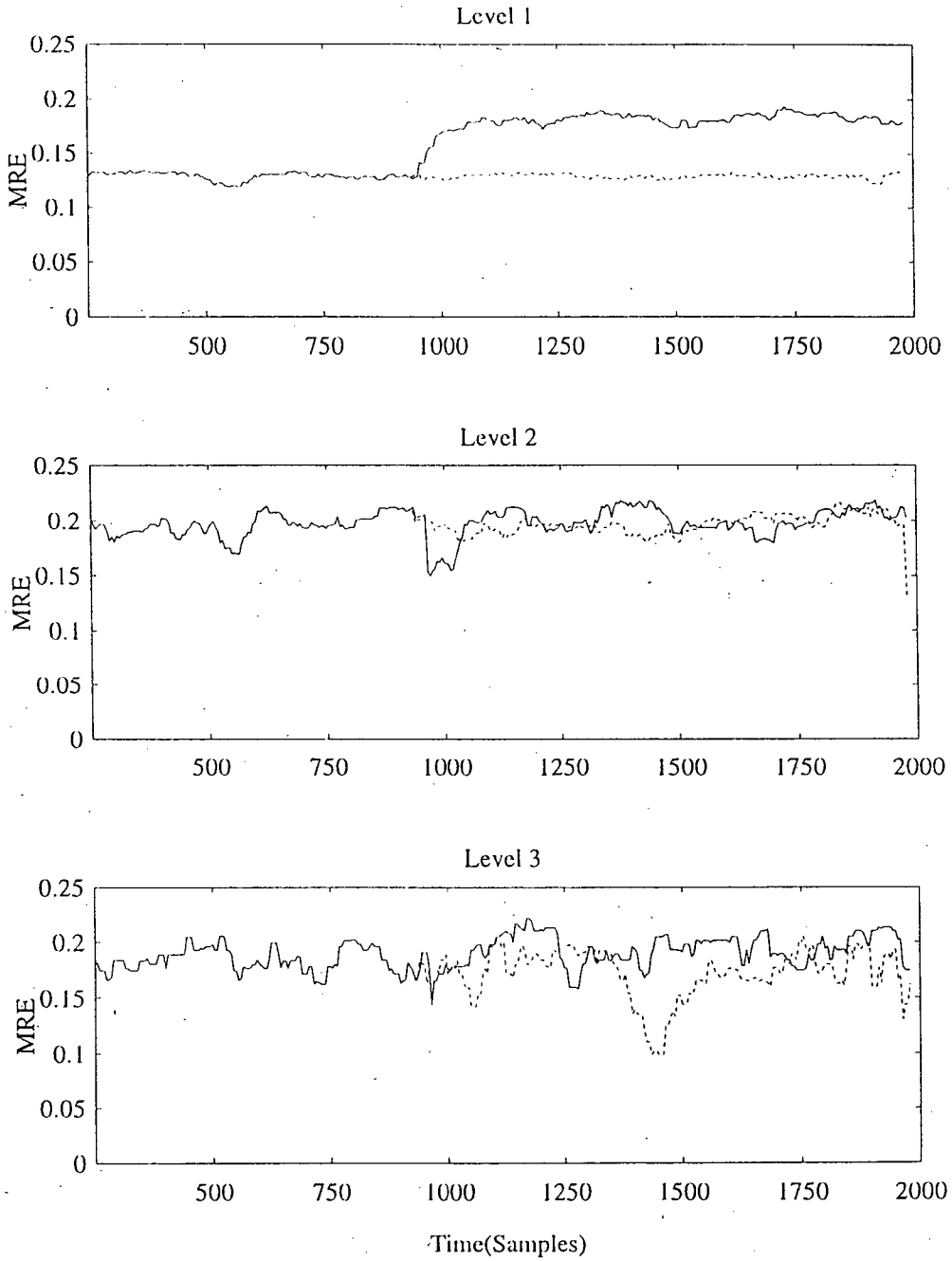

FIG. 4. Henon Map. Temporal evolution of Shannon's Entropy for the first state of Eq. (122) with fixed parameters (dashed line) vs. that obtained for the signal with a variable parameter (full line) (See Figure 1).

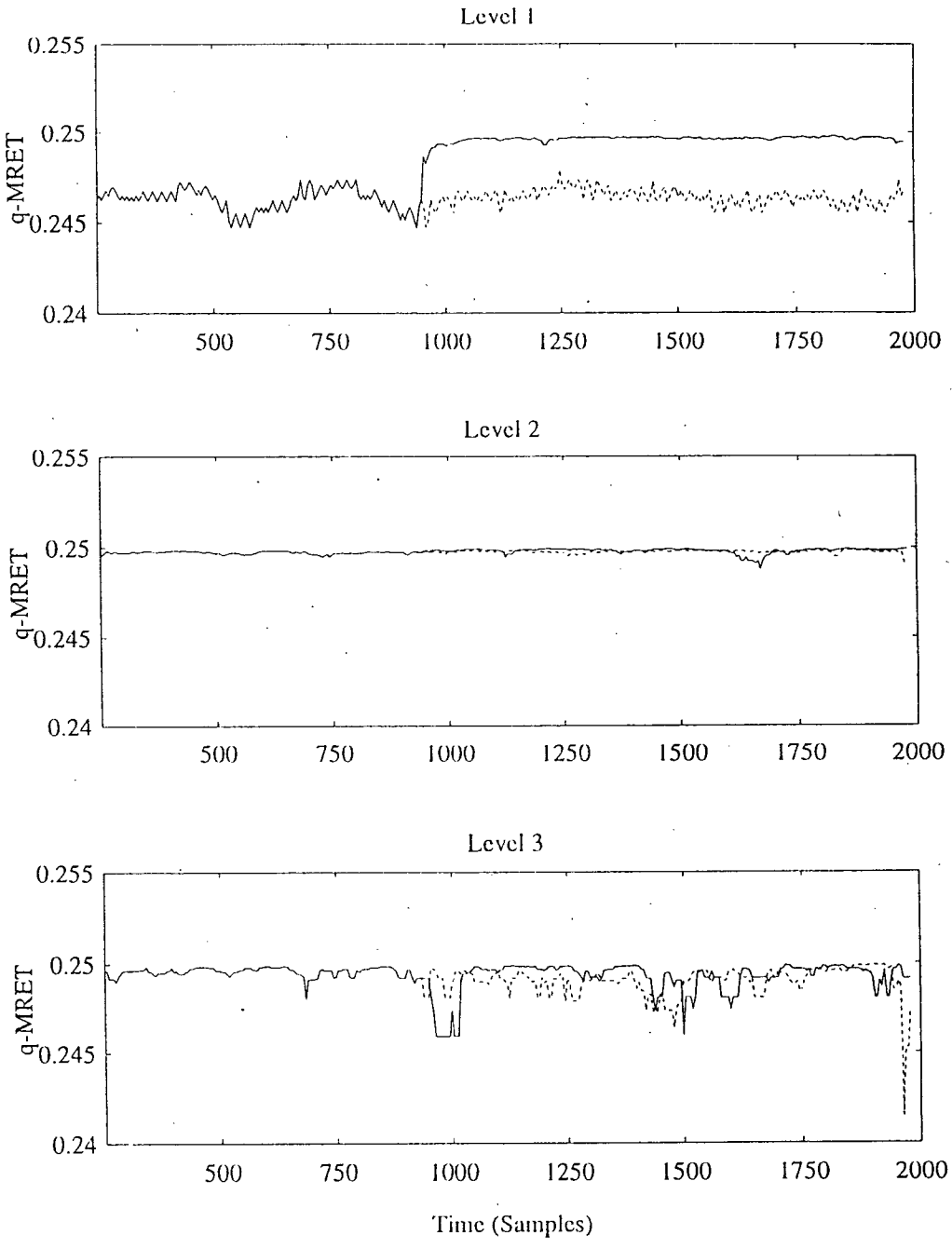

FIG. 5. Henon Map. Temporal evolution of the three first resolution levels of Shannon based Multiresolution Entropy for the first state of Eq. (122) with fixed parameters (dashed line) vs. that obtained for the signal with a variable parameter (full line). (See Fig. 1).

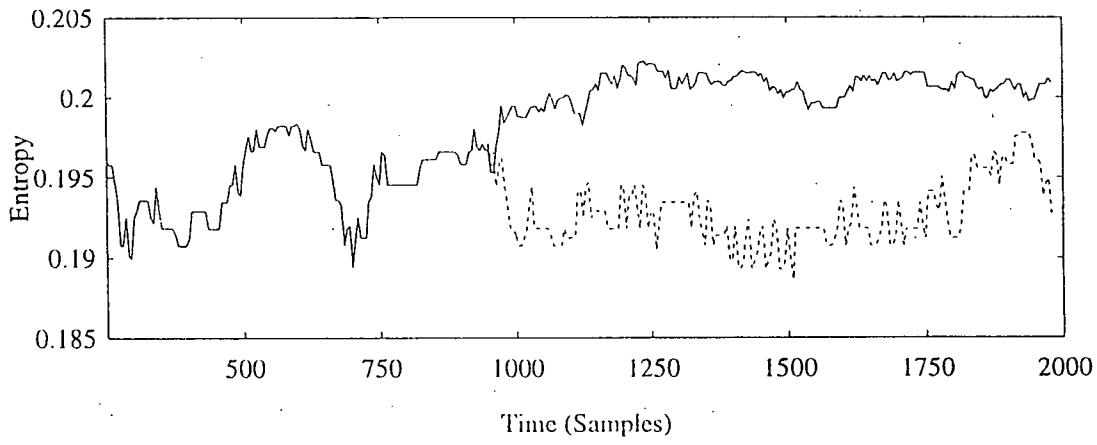

FIG. 6. Lorenz equations. Temporal evolution for the second state of Eq. (125), solved by resource of the fourth order Runge-Kutta method, with a step $\Delta\ t\ =\ 0.01$ and initial values $x(0)\ =\ 10$, $y(0)\ =\ 1$, $z(0)\ =\ 0$. The dashed line corresponds to a fixed parameters-model and the full line to a variable parameter-model, according to Eq.(123).

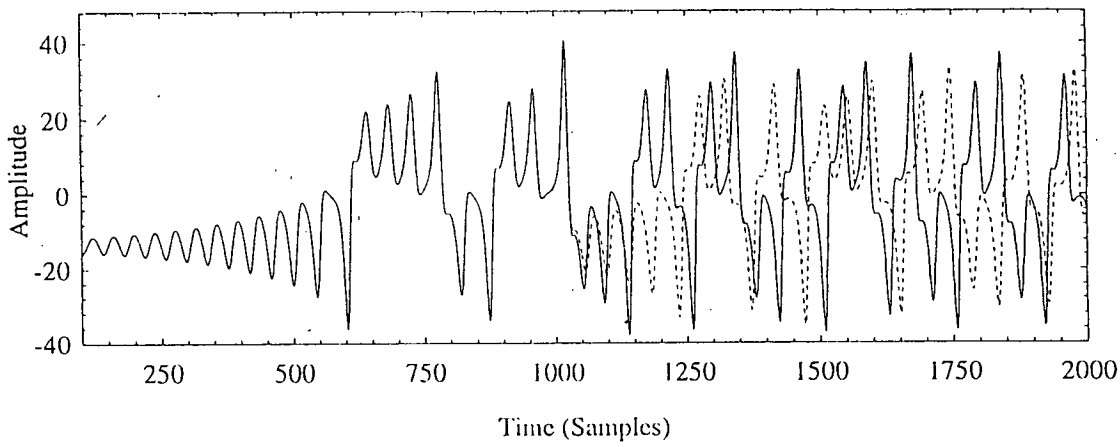

FIG. 7. Lorenz equations. In the case of the signals depicted in Fig. 6 we plot the temporal evolution of the $q\ =\ 5$-Tsallis entropy. Additional details are as in Fig. 6.

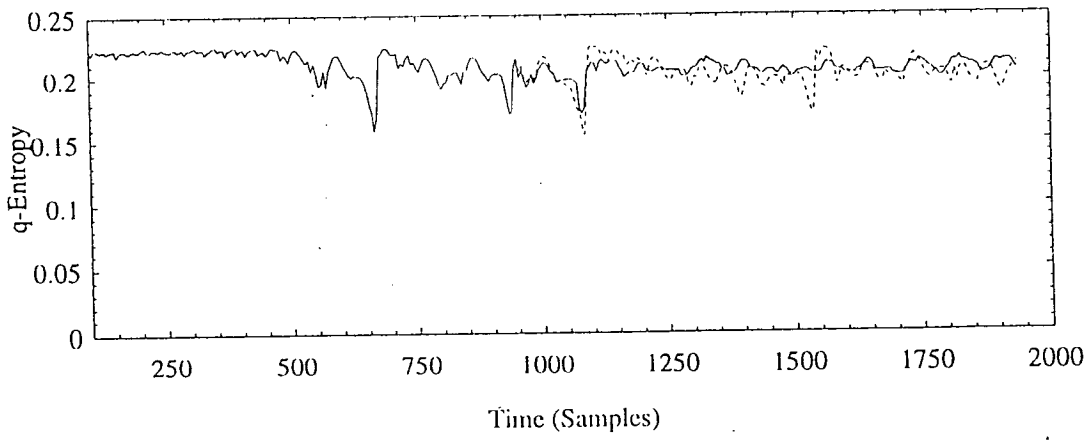

FIG. 8. Lorenz equations. Temporal evolution of the $q = 5$-Tsallis multiresolution entropy evaluated for the signals displayed in Fig. 6. For additional details, see the corresponding figure's caption.

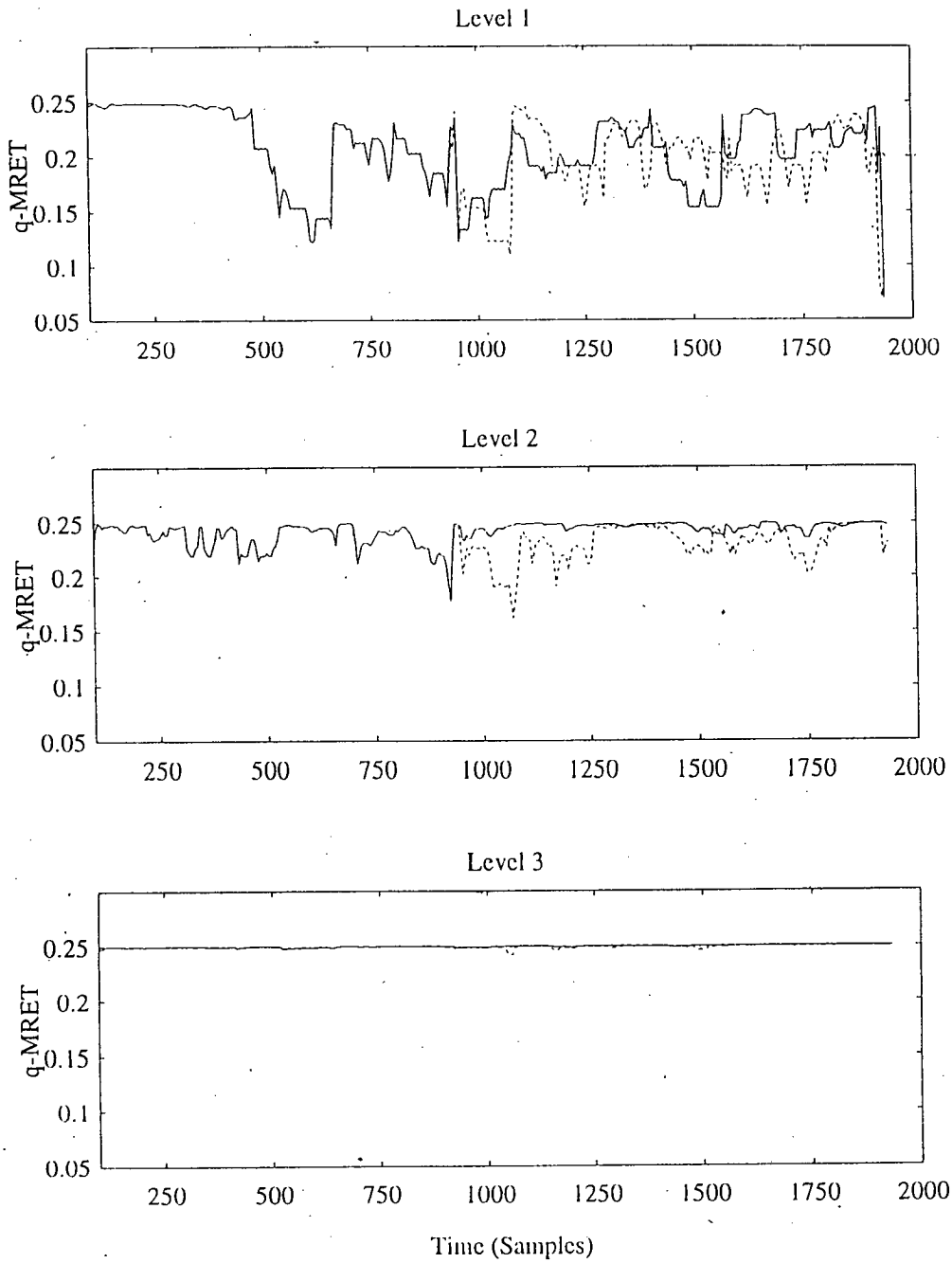

FIG. 9. Lorenz equations. Graph of Shannon's entropy temporal evolution of the signals depicted in Fig. 6, where additional details should be consulted.

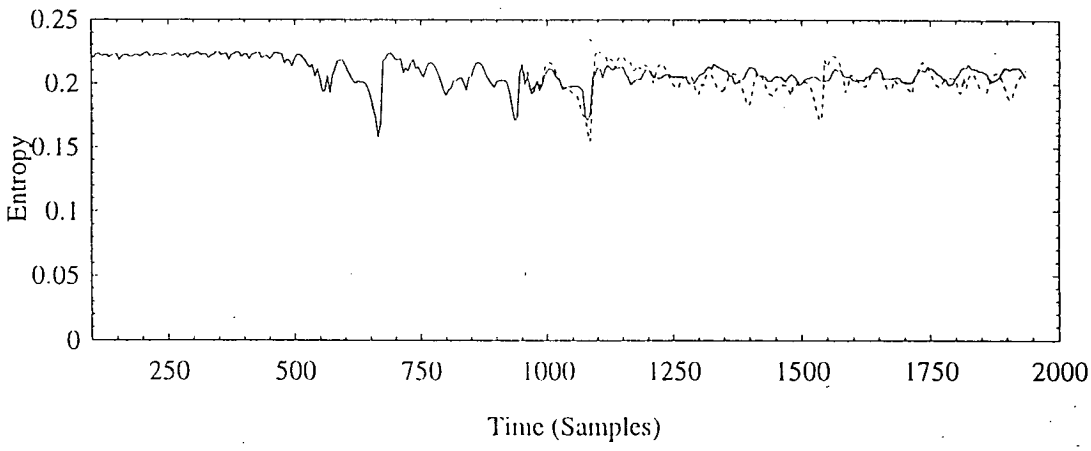

FIG. 10. Lorenz equations. Shannon's multiresolution entropy temporal evolution. Signals are that portrayed in Fig. 6, where additional details should be consulted.

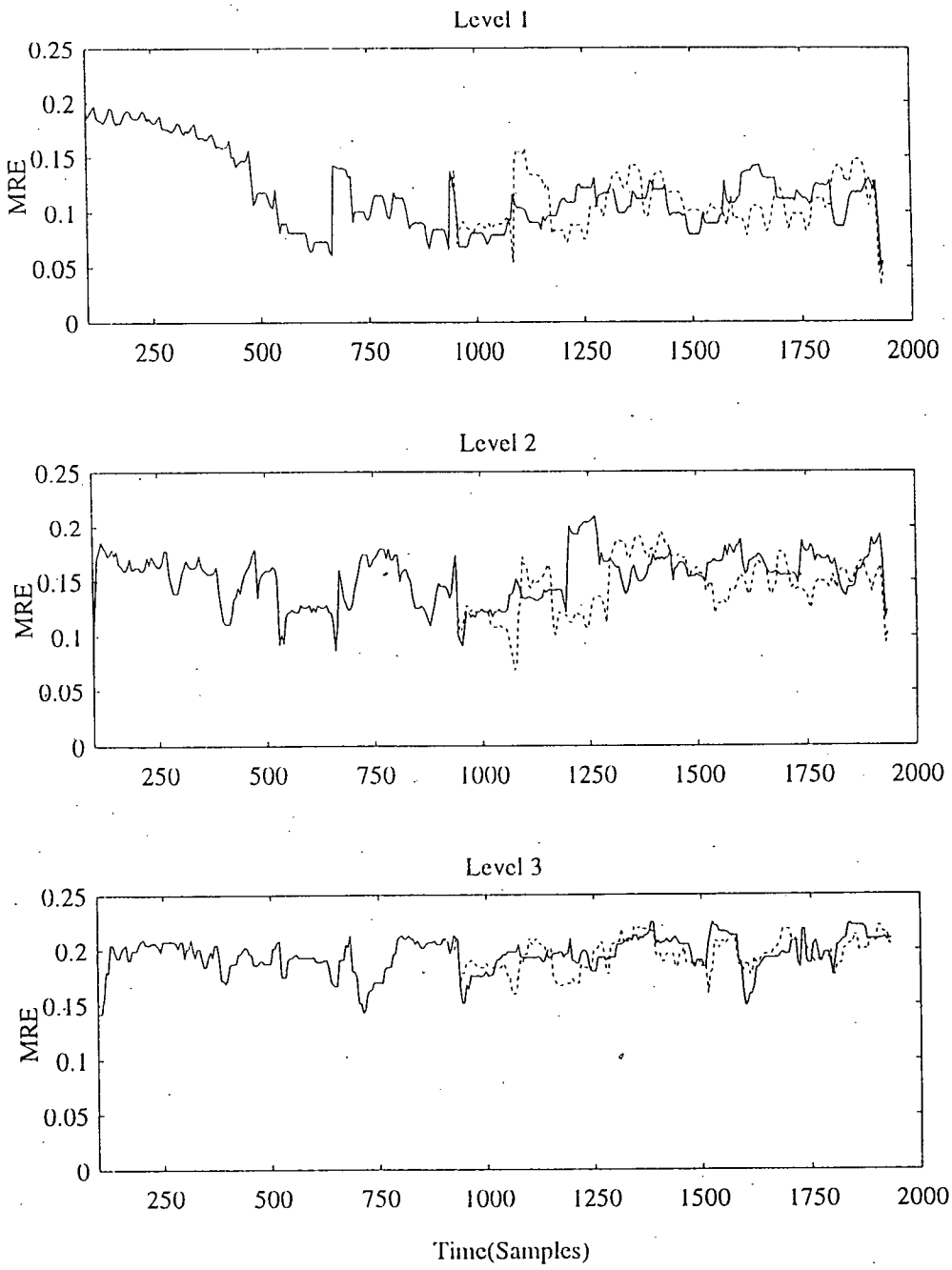

FIG. 11. A 20 s EEG turtle's signal (sample frequency 200 Hz, low pass filter at 100 Hz). a) segment without LSW. b) segment with LSW in sample around 2000.

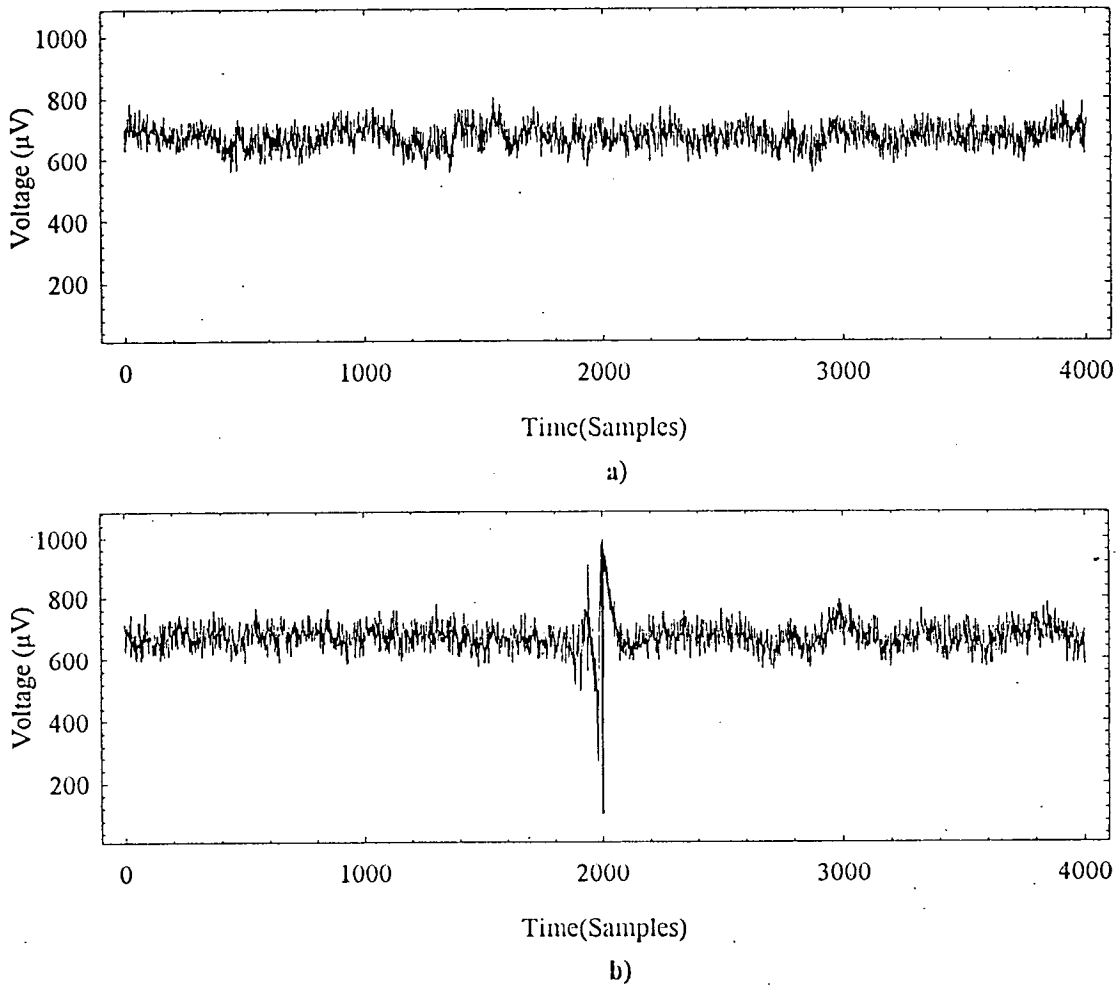

FIG. 12. Turtle's EEG wavelet decomposition. Turtle's EEG shown at Fig. 11 wavelet decomposition ; frequency ranges at each level are printed above each plot. a) Segment without LSW. b) Segment with LSW. The LSW has components at all wavelet levels.

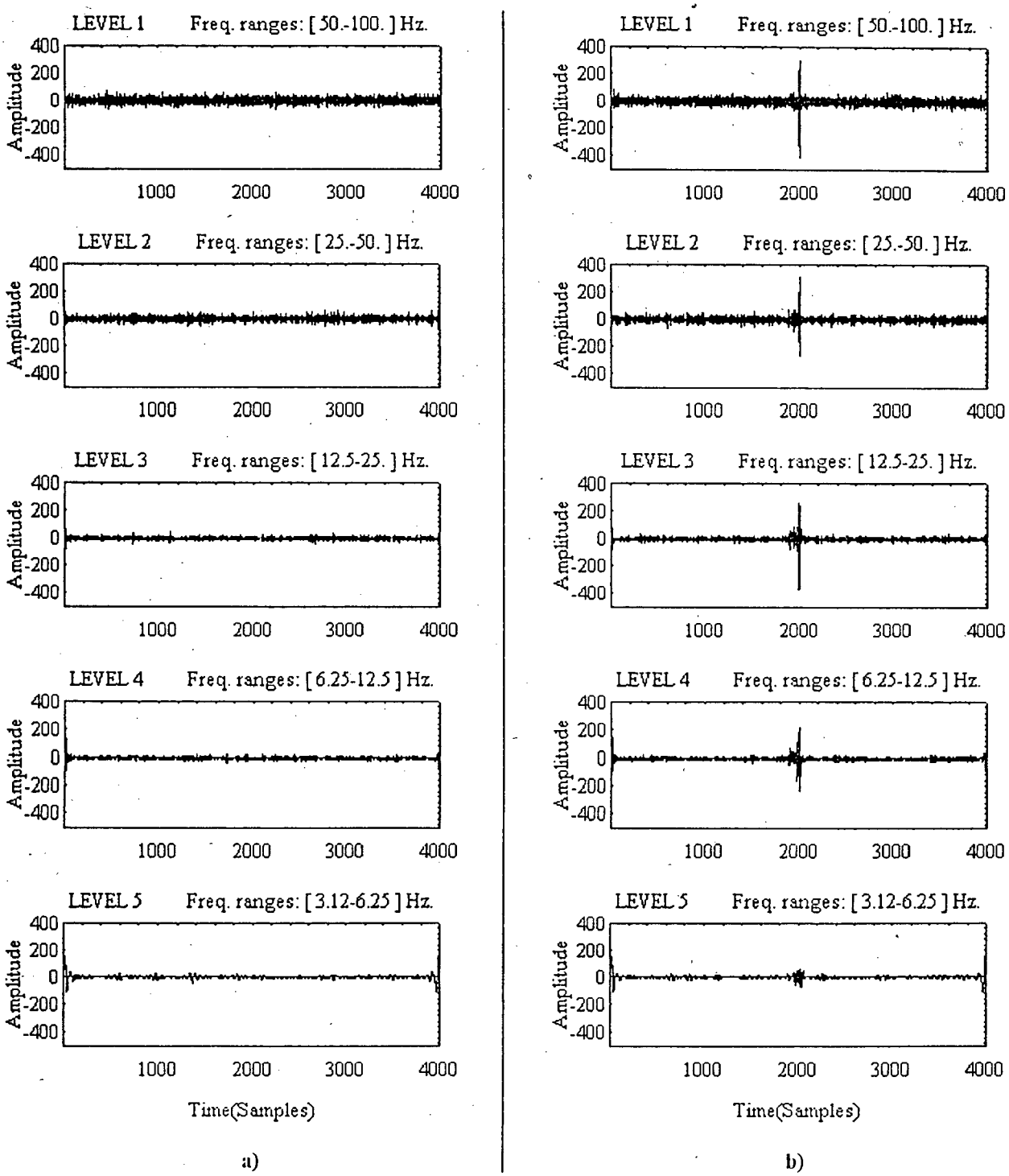

FIG. 13. Spectrogram of the same signals shown in Fig. 11. Sample frequency 200 Hz, low pass filter at 100 Hz. a) segment without LSW. b) segment with LSW. Note that the area within (0-15 Hz) enhances,in the segment of signal with the LSW in comparison to the segment without LSW.

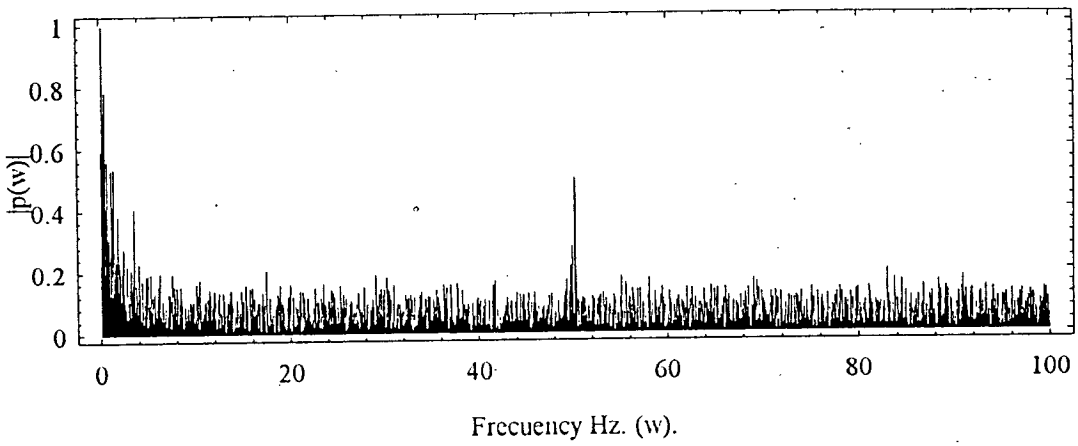

a)

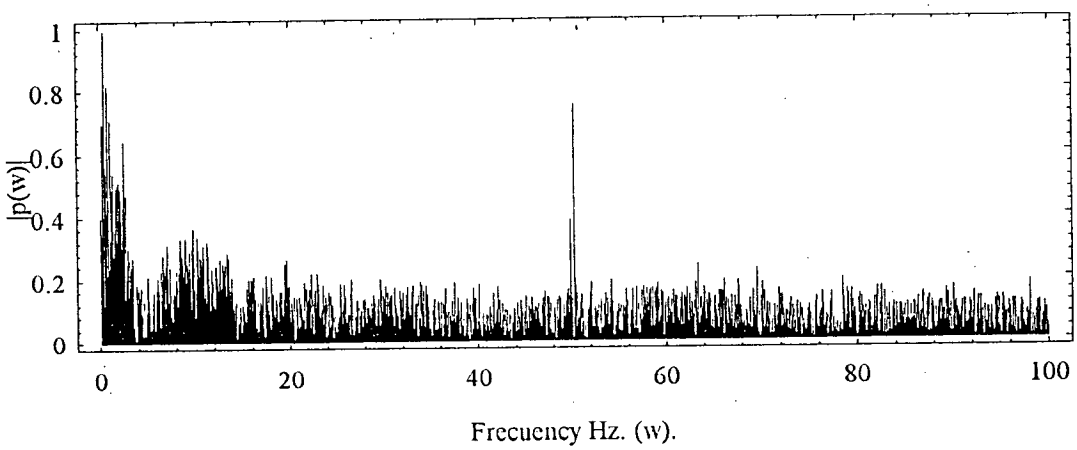

b)

FIG. 14. Shannon's entropy evolution of the signal shown at Fig. 11-b. The entropy has been calculated with 128 samples windows. a) Shannon's entropy evolution of the original signal. b) Shannon's entropy evolution of the signal's derivative. c) Tsallis's entropy evolution of the original signal. Note that the relation between the amplitudes of the entropy fall during the EFS and the amplitudes of the entropy oscillations in the background of the EEG without LSW, is greater than Fig. 14-a. d) Tsallis's entropy evolution of the signal's derivative. The magnitude of the fall is enhanced and no additional falls are introduced.

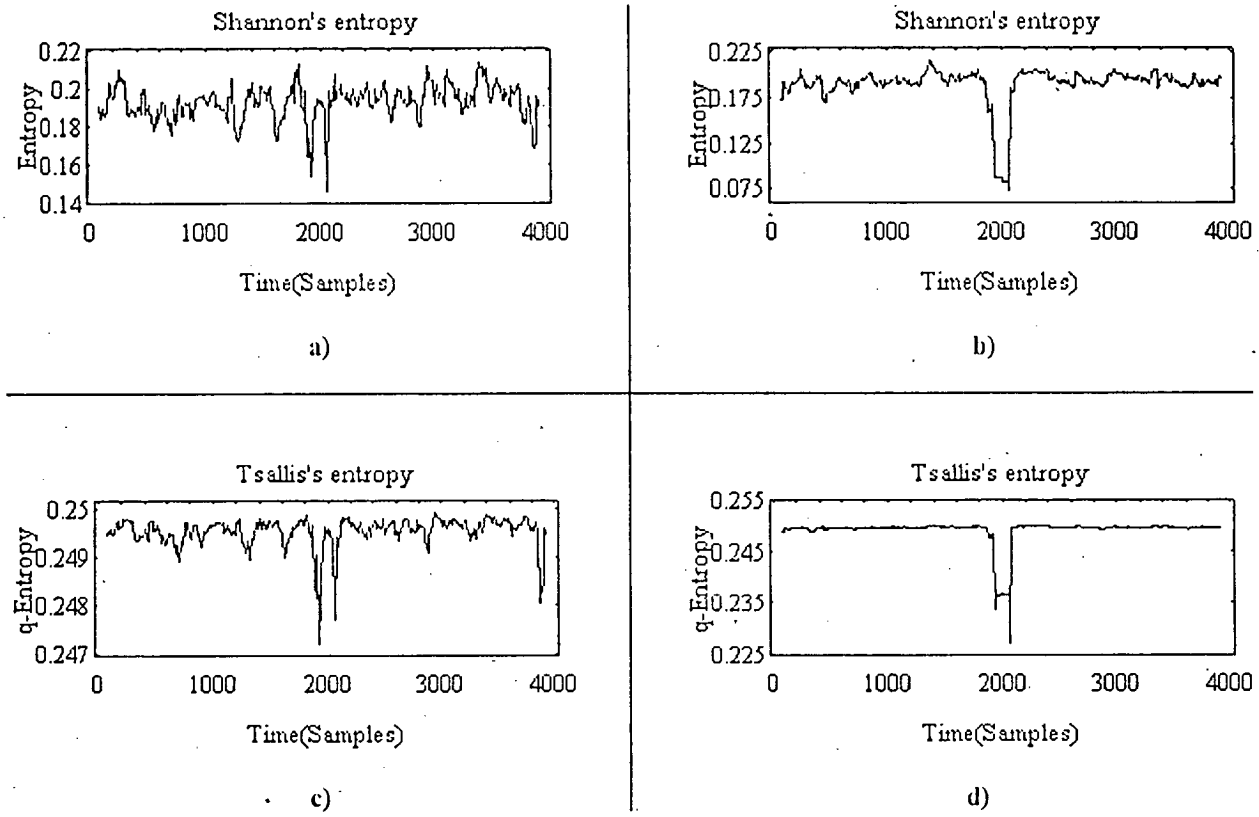

FIG. 15. Multiresolution entropy of the signal shown at Fig. 11-b. The entropy has been calculated with 128 samples windows. a) MRE of the original signal. b)MRE of the signal's derivative. c) MRET of the original signal. d) MRET of the signal's derivative.

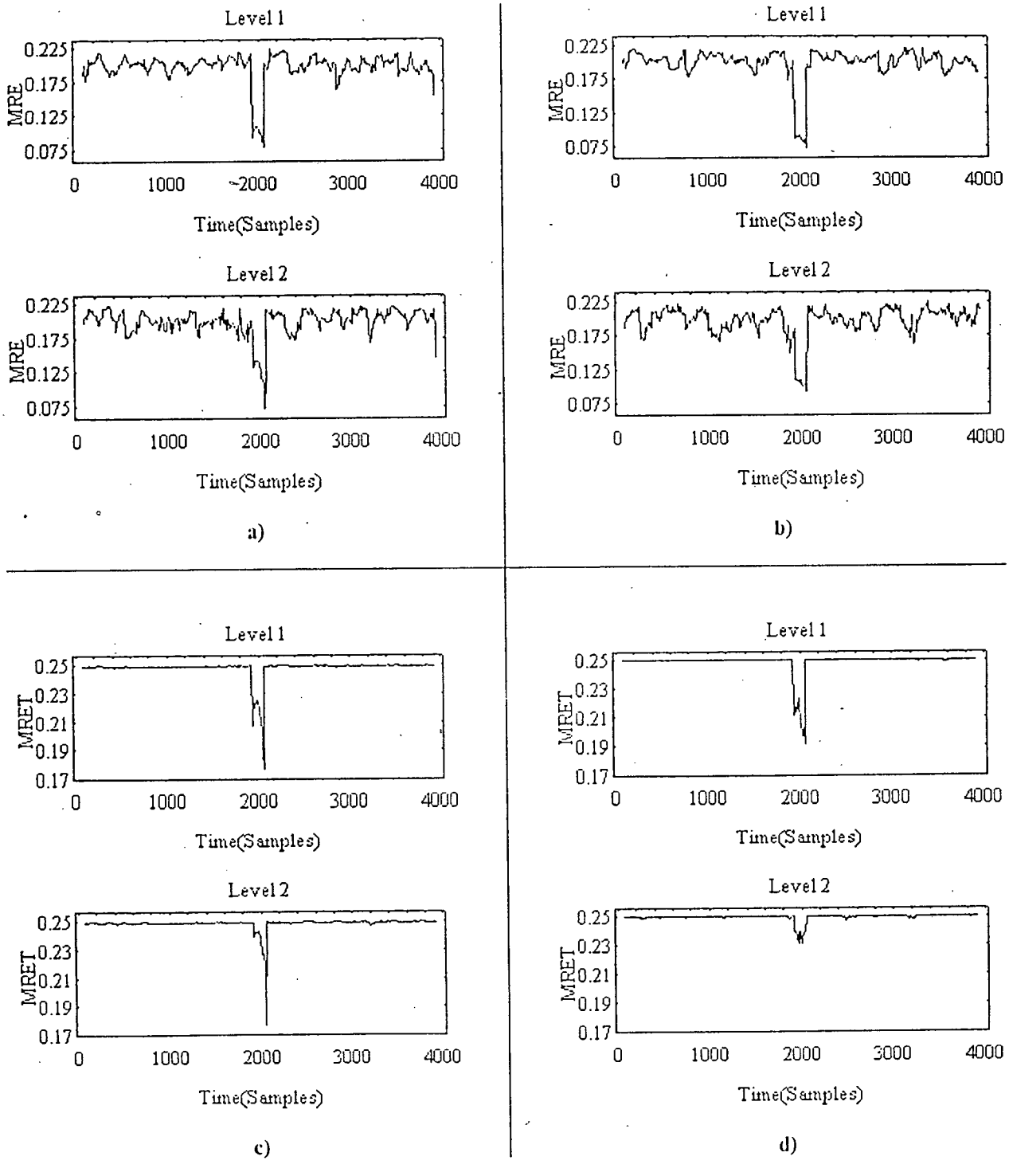

FIG. 16. Human EEG. A 50 sec. EEG signal of a patient with focal epilepsy. Sample frequency 102.5 Hz ; low pass filter at 51.25 Hz. a) segment without LSW. b) segment with LSW in samples between (0-800).and (3800-4500).

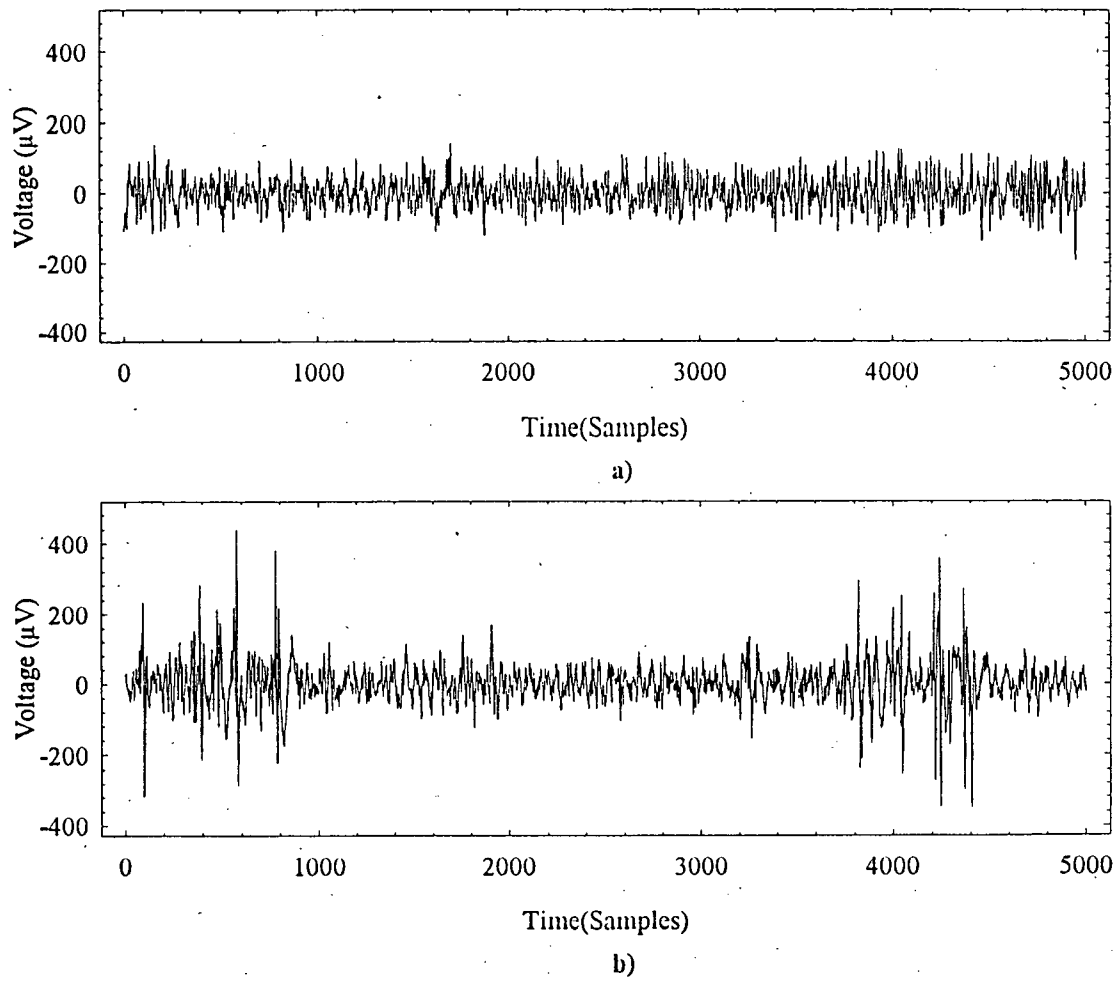

FIG. 17. Wavelet decomposition of the EEG shown at Fig. 16; frequency ranges at each level are printed above each trace. a) segment without LSW. b) segment with LSW. Note that the LSW appears at levels $W_2 - W_6$.

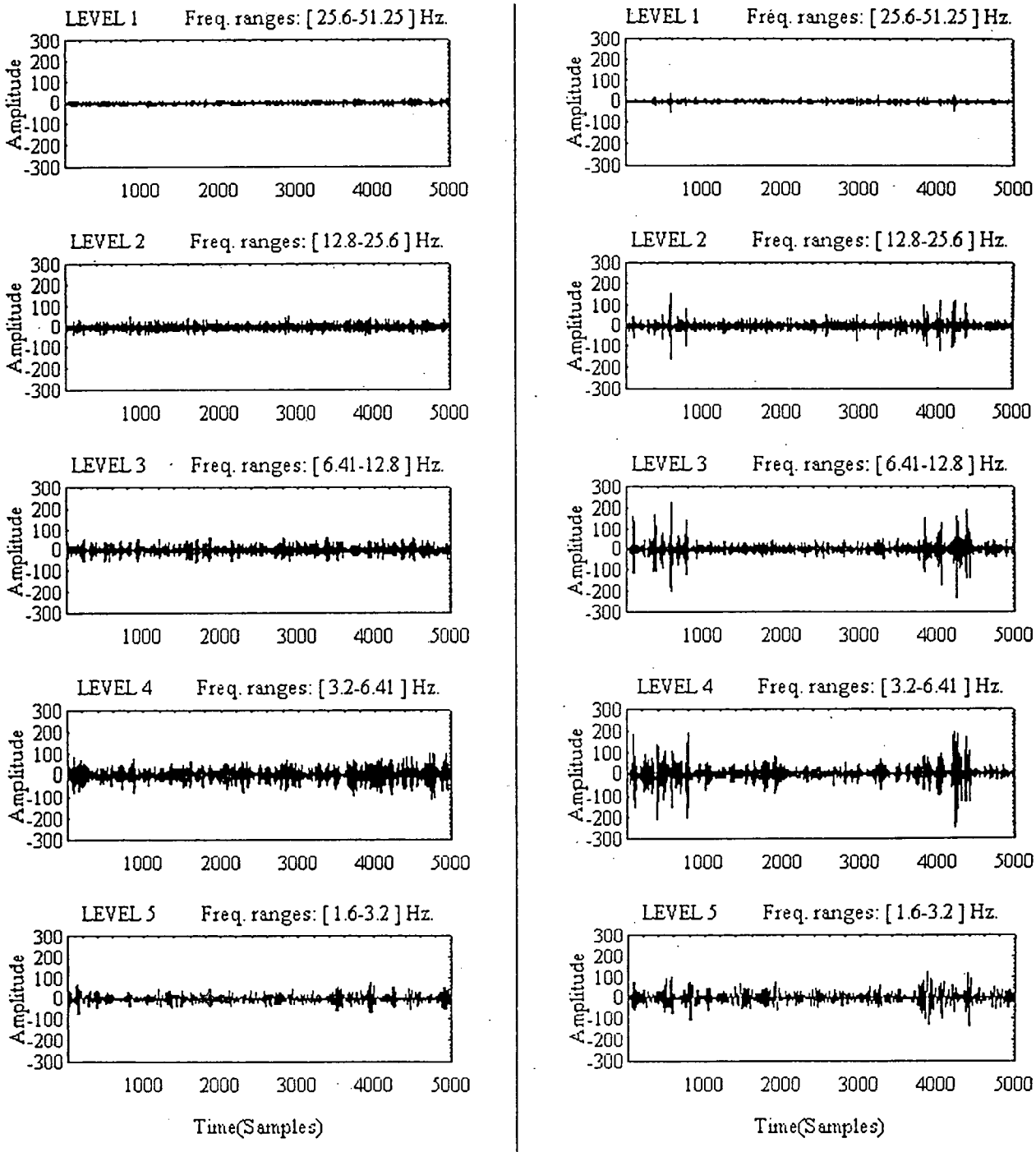

FIG. 18. Entropy evolution of the signal shown at Fig. 16-b. The entropy has been calculated with 128 samples windows. a)Shannon's entropy evolution of the original signal. b) Shannon's entropy evolution of the signal derivative. (Note that the LSW can be detected with more clarity than at Fig. 18-a.) c) Tsallis's entropy evolution of the original signal. d) Tsallis's entropy evolution of the signal derivative.

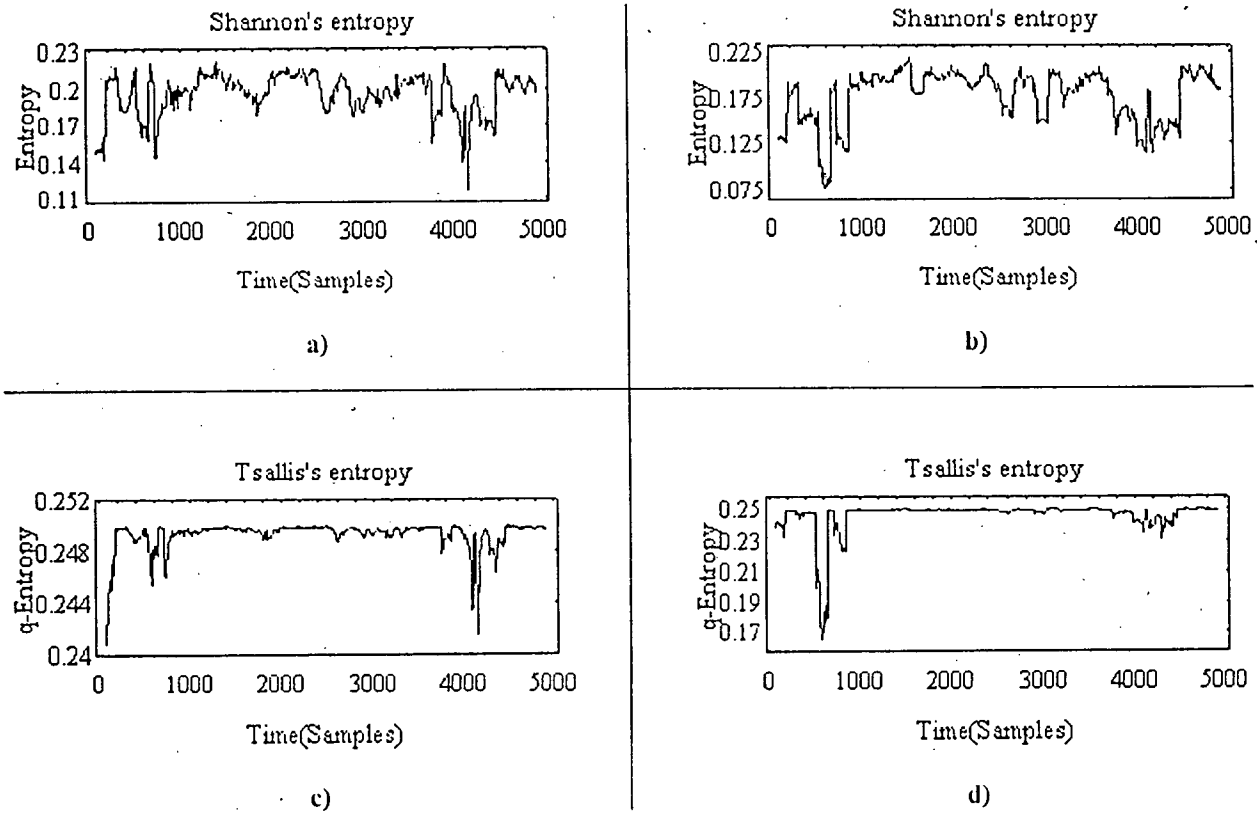

FIG. 19. Multiresolution entropy of the signal shown at Fig. 16-b. The entropy has been calculated with 128 samples windows. a) MRE of the original signal. b) MRE of the signal's derivative. c) MRET of the original signal. d) MRET of the signal's derivative.

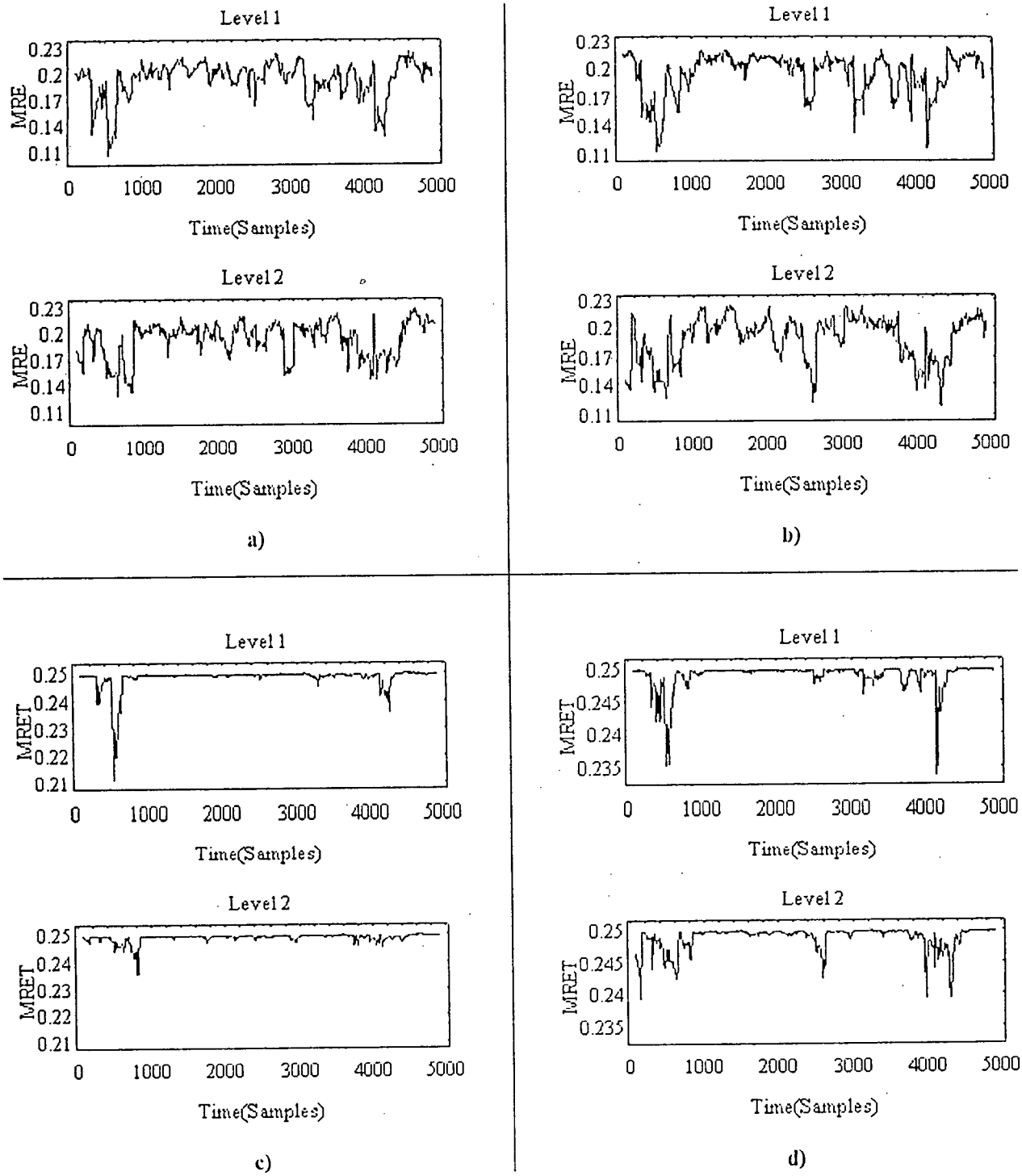

TABLES

A)

frecuency interval	37.5 - 150 Hz. *		4.69 - 37.5 Hz.	
signal	nosw	wsw	nosw	wsw
area	$0.33\pm6.4 \times 10^{-4}$	$0.23\pm3.92 \times 10^{-3}$	$0.49\pm3.66 \times 10^{-3}$	$0.50\pm5.44 \times 10^{-3}$
significant level	$p=2.63 \times 10^{-3}$		p=0.93	

frecuency interval	0.58 - 4.69 Hz. *	
signal	nosw	wsw
area	$0.13\pm2.9 \times 10^{-4}$	$0.24\pm2.35 \times 10^{-3}$
significant level	$p=1.30 \times 10^{-4}$	

B)

wavelet level	W1*		W2		W3	
signal	nosw	wsw	nosw	wsw	nosw	wsw
energy	$0.03\pm1.2\times10^{-4}$	$0.01\pm4.\times10^{-5}$	$0.03\pm1.1\times10^{-4}$	$0.02\pm2.3\times10^{-4}$	$0.12\pm1.6\times10^{-3}$	$0.11\pm2.26\times10^{-3}$
significant level	$p = 5.92 \times10^{-3}$		p = 0.43		p = 0.87	

wavelet level	W4		W5		W6*	
signal	nosw	wsw	nosw	wsw	nosw	wsw
energy	$0.21\pm1.11\times10^{-2}$	$0.19\pm6.1\times10^{-3}$	$0.11\pm1.51\times10^{-3}$	$0.15\pm2.87\times10^{-3}$	$0.11\pm1.2\times10^{-3}$	$0.21\pm6.08\times10^{-3}$
significant level	p = 0.68		p = 0.14		$p = 1.04 \times10^{-2}$	

(nosw = no sharp wave ; wsw = with sharp wave)

TABLE I. A) Statistics comparison (means (STD)) of relative Fourier areas between 10 segments without LSW and with LSW, taken from 5 turtles (sample rate 300 Hz, low pass filter at 150 Hz). The differences with $P \leq 0.05$ are indicated with an asterisk. B) Statistics comparison (means (STD)) of relative wavelet coefficients energy of 10 segments (without LSW and with LSW), taken from 5 turtles (sample rate 300 Hz, low pass filter at 150 Hz). The differences with $P \leq 0.05$ are indicated with an asterisk.

TABLE II. A) Statistics comparison of relative wavelet coefficients' energy of 20 segments (without EFS and with EFS), taken from 10 patients (sample rate 102.5 Hz, low pass filter at 51.25 Hz). The differences with $P \leq 0.05$ are indicated with an asterisk. B) Statistics comparison of relative Fourier areas of 10 segments (without EFS and with EFS), taken from 5 turtles (sample rate 300 Hz, low pass filter at 150 Hz).The differences with $P \leq 0.05$ are indicated with an asterisk.

A)

wavelet level	W1*		W2*		W3	
signal	nosw	wsw	nosw	wsw	nosw	wsw
energy	0.04±0.002	0.01±0.0001	0.14±0.001	0.10±0.001	0.28±0.002	0.30±0.07
significant level	p=1.8 x10^{-2}		p=1.75 x10^{-3}		p= 3.77x10^{-1}	

wavelet level	W4		W5		W6	
signal	nosw	wsw	nosw	wsw	nosw	wsw
energy	0.30±0.004	0.31±0.004	0.17±0.003	0.21±0.003	0.064±0.001	0.058±0.001
significant level	p=7.40 x10^{-1}		p=4.51 x10^{-2}		p=5.24 x10^{-1}	

W1 + W2*	
nosw	wsw
0.18±0.004	0.11±0.002
p=1.17x10^{-3}	

W3 + W4 +W5*	
nosw	wsw
0.76±0.003	0.83±0.004
p=2.16x10^{-3}	

W3 + W4 + W5 + W6*	
nosw	wsw
0.82±0.002	0.88±0.002
p=2.30x10^{-4}	

B)

frecuency interval	0 - 12.8 Hz. *		12.8 - 50 Hz. *	
signal	nosw	wsw	nosw	wsw
area	0.65±0.001	0.74±0.003	0.34±0.001	0.25±0.003
significant level	p=2.35 x 10^{-6}		p=2.09 x 10^{-6}	

(nosw = no sharp wave ; wsw = with sharp wave)

TABLE III. A) Statistics comparison of relative Fourier areas of the derivative of the same signals shown at Table IIA and Table IIB. The differences with $P \leq 0.05$ are indicated with an asterisk. B) Statistics comparison of relative wavelet energy of the derivative of the same signals shown at Table IIA and Table IIB. The differences with $P \leq 0.05$ are indicated with an asterisk.

A)

frecuency levels	3.2 - 12.8 Hz. *		25.62 - 50 Hz. *	
signal	nosw	wsw	nosw	wsw
area	0.27±0.001	0.38±0.006	0.34±0.002	0.25±0.003
significant level	$p=2.0 \times 10^{-5}$		$p=3.0 \times 10^{-5}$	

B)

wavelet level	W1*		W2		W3*	
signal	nosw	wsw	nosw	wsw	nosw	wsw
energy	0.30±0.003	0.16±0.006	0.40±0.003	0.38±0.007	0.22±0.003	0.35±0.015
significant level	$p=2.36 \times 10^{-6}$		$p=4.18 \times 10^{-1}$		$p=5.7 \times 10^{-6}$	

wavelet level	W4*		W5		W6	
signal	nosw	wsw	nosw	wsw	nosw	wsw
energy	0.07±0.001	0.10±0.001	$0.011 \pm 1 \times 10^{-5}$	$0.014 \pm 6 \times 10^{-5}$	0.0	0.0
significant level	$p=8.69 \times 10^{-3}$		$p=1.03 \times 10^{-1}$			

(nosw = no sharp wave ; wsw = with sharp wave)

W1 + W2*	
nosw	wsw
0.69±0.005	0.53±0.020
$p=2.80 \times 10^{-4}$	

W3 + W4*	
nosw	wsw
0.29±0.005	0.45±0.020
$p=4.2 \times 10^{-4}$	

Unité de recherche INRIA Rocquencourt
Domaine de Voluceau - Rocquencourt - B.P. 105 - 78153 Le Chesnay Cedex (France)

Unité de recherche INRIA Lorraine - Technopôle de Nancy-Brabois - Campus scientifique
615, rue du Jardin Botanique - B.P. 101 - 54602 Villers lès Nancy Cedex (France)
Unité de recherche INRIA Rennes - IRISA, Campus universitaire de Beaulieu 35042 Rennes Cedex (France)
Unité de recherche INRIA Rhône-Alpes 46, avenue Félix Viallet - 38031 Grenoble Cedex 1 (France)
Unité de recherche INRIA Sophia Antipolis - 2004, route des Lucioles - B.P. 93 - 06902 Sophia Antipolis Cedex (France)

Éditeur
INRIA - Domaine de Voluceau - Rocquencourt - B.P. 105 - 78153 Le Chesnay Cedex (France)

ISSN 0249 - 6399